The Nature and Absolute Hydration Free Energy of the Solvated Electron in Water

Chang-Guo Zhan*,† and David A. Dixon*,‡

William R. Wiley Environmental Molecular Sciences Laboratory, Pacific Northwest National Laboratory, MS K1-83, P.O. Box 999, Richland, Washington 99352

Received: October 29, 2002; In Final Form: February 3, 2003

We report the first first-principles solvation-included electronic structure study to energetically compare a variety of candidate structures of the hydrated electron and to determine its absolute hydration free energy $\Delta G_{hyd}^{298}(e^-)$. The calculated results show that both the thermal motion and bulk solvent effects can qualitatively change the relative thermodynamic stability of different structures of the hydrated electron on the basis of a cluster of a given size, and that the most stable structure in solution is not necessarily the most stable one in the gas phase. For a given number of explicitly included solvent water molecules, the most stable structure in solution reveals a unique feature of the chemical nature of the solvated electron in water, i.e., the electron forms two strong electron−hydrogen bonds of the $e^-\cdots HO$ type with the hydrogen-bonded water cluster and two of the hydrogen bonds in the neutral water cluster are broken. On the basis of the most stable structures, the calculated electronic excitation energies are within the observed absorption range of the hydrated electron in water. The absolute hydration free energy of the solvated electron in water has been calculated to be −35.5 kcal/mol by using a reliable computational protocol of first-principles solvation-included electronic structure calculations. This value is in excellent agreement with a recently obtained value of −34.6 kcal/mol. The predicted $\Delta G_{hyd}^{298}(e^-)$ value of −35.5 kcal/mol, when combined with our previously predicted $\Delta G_{hyd}^{298}(H^+)$ value of −262.4 kcal/mol and $\Delta G_{hyd}^{298}(HO^-)$ value of −104.5 kcal/mol by using the same computational protocol, gives $\Delta G_{hyd}^{298}(e^-) + \Delta G_{hyd}^{298}(H^+) = -297.9$ kcal/mol and $\Delta G_{hyd}^{298}(e^-) - \Delta G_{hyd}^{298}(HO^-) = 69.0$ kcal/mol, in excellent agreement with the corresponding values derived from experimental data.

Introduction

The solvated electron in aqueous solution can be generated by radiolysis or photolysis of liquid water[1] and has distinctive properties including a broad and intense photoabsorption spectrum,[2] a high diffusion rate, and a high reactivity.[3−5] However, despite extensive experimental and computational studies, the microscopic structure of the solvated electron in water remains an enigma. Numerous experimental measurements with high time-resolution have yielded a wealth of data on the mechanism of formation of the hydrated electron and on its spectroscopic properties, without providing definitive results as to what the structure of the equilibrated solvated electron in water may be.[6−21] Nevertheless, a number of candidate structures have been proposed in the literature. A qualitative picture of the hydrated electron is that a localized electronic charge distribution exists in a cavity of the hydrogen-bonded network of water molecules with varying coordination numbers.[22−28] Alternative structural descriptions of the hydrated electron include the $(OH^-\cdots H_3O)(aq)$ type of complex and its variants.[29−33] As we do not yet know the structure of the solvated electron in aqueous solution, the exact chemical nature of the hydrated electron and the mechanisms of its reactions with other species are not well understood at the molecular level, even though experimental rate constants and activation energies are available for over a thousand chemical reactions of the hydrated electron.[5]

A key to understanding the equilibrium thermodynamic properties of the chemical reactions of the hydrated electron is the value of its absolute solvation free energy in water $\Delta G_{hyd}^{298}(e^-)$. However, the exact value of this important quantity remains unknown because the absolute hydration free energy of a charged species is inherently difficult to determine by experiment. Jortner and Noyes[34] estimated the $\Delta G_{hyd}^{298}(e^-)$ value to be −39.4 kcal/mol on the basis of extrapolating results for monatomic cations.[35] By using data from Shiraishi et al.[36] and an extrapolation approach developed and described by Coe,[37] Bartels[38] gives a value of −34.6 kcal/mol for the free energy of solvation of the electron. As any stable, macroscopic solution contains equal amounts of positive and negative charge,[39,40] without using additional approximations or models, an experiment can only be performed to determine the sum of hydration free energies of a pair of oppositely charged species. It has not yet been possible to isolate one type of charged species and measure its absolute solvation free energy. Hence, direct experimental data for different pairs of charged species can provide information only for the relative magnitudes of the ionic/electronic hydration free energies.[41−43] Thus, it is not surprising to find that the reported "experimental" absolute hydration free energy of the proton $\Delta G_{hyd}^{298}(H^+)$ has a wide range from −252.6 to −264.1 kcal/mol[44] and that of hydroxide ion $\Delta G_{hyd}^{298}(HO^-)$ has an even wider range from −90.6[45] to −110.0 kcal/mol.[46]

Reliable first-principles computational approaches can be used to complement experimental studies for determining the equilibrium structure and absolute hydration free energy of the solvated electron in water. Recent molecular dynamics and Monte Carlo simulations describe the dynamics of a quantum mechanical electron in a classical water environment or describe electron(s) existing in a gas-phase water cluster (quantum

* To whom correspondence should be addressed.
† E-mail: chang-guo.zhan@pnl.gov.
‡ E-mail: david.dixon@pnl.gov.

10.1021/jp022326v CCC: $25.00
Published on Web 04/05/2003

dynamics).[27,28,47−87] Ab initio quantum mechanical studies of the hydrated electron reported so far have been limited to calculations on gas-phase clusters,[33,88−103] which complement the corresponding experimental studies of the gas-phase clusters.[104−119] No first-principles electronic structure calculations have been performed to identify the most stable structure of the solvated electron in water by accounting for the bulk solvent effects or to determine the absolute hydration free energy of the solvated electron on the basis of first-principles electronic structure calculations that we are aware of.

Recently, we have developed a hybrid supermolecule-continuum approach[120−122] in which part of the solvent surrounding the solute is treated quantum mechanically at a high level and the remaining bulk solvent is approximated by a dielectric continuum medium model. We employ a recently developed self-consistent reaction field model known as the surface and volume polarization for electrostatic interaction (SVPE)[123−126] or the fully polarizable continuum model (FPCM).[120,127−129] With this approach, the calculated results can systematically be improved and converged by increasing the number of explicit solvent molecules included in the quantum chemical calculation. This approach has been employed to predict activation energies for ion−molecule reactions[120] and absolute hydration free energies of ions[121,122] with high accuracy. For example, the $\Delta G_{hyd}^{298}(H^+)$, $\Delta G_{hyd}^{298}(Li^+)$, and $\Delta G_{hyd}^{298}(HO^-)$ values have accurately been predicted to be −262.4, −125.1, and −104.5 kcal/mol, respectively.[121,122] The predicted absolute hydration free energy shift (137.3 kcal/mol) from the proton to Li^+ is in excellent agreement with the corresponding experimental shift, 137.5 kcal/mol, based on the latest collection of experimental data,[42] and 137.0 kcal/mol, based on the earlier experimental data.[45] The predicted $\Delta G_{hyd}^{298}(HO^-)$ and $\Delta G_{hyd}^{298}(H^+)$ values allow the prediction of the sum of absolute hydration free energies of the proton and hydroxide to be −366.9 kcal/mol, in excellent agreement with the experimental thermodynamic values of −367.1 ± 0.2 kcal/mol (based on the NIST gas-phase experimental value[130]) and −366.6 ± 0.1 kcal/mol (based on a very recently revised gas-phase experimental value for $\Delta H_f(OH)$[131,132]).

On the basis of the success of the SVPE-based supermolecule-continuum calculations for the absolute hydration free energies of ions, we have used it to study possible stable structures of the hydrated electron and to determine its absolute hydration free energy $\Delta G_{hyd}^{298}(e^-)$. On the basis of the most stable structure in solution, we provide insight into the chemical nature of the solvated electron in water. In addition, electronic excitation energies have been calculated and compared with the reported experimental observations. With an accurately determined $\Delta G_{hyd}^{298}(e^-)$ value, together with the previously calculated $\Delta G_{hyd}^{298}(H^+)$ and $\Delta G_{hyd}^{298}(HO^-)$ values by using the same computational protocol, we can directly compare the first-principles prediction with available experimental thermodynamic data involving the hydrated electron.

Computational Methods

The general hybrid supermolecule-continuum approach to the absolute hydration free energy of a charged species has been described elsewhere in detail.[121,122] The physical meaning of such a hybrid supermolecule-continuum approach, i.e., performing a self-consistent reaction field (SCRF) calculation on the supermolecular solute, is that the part of the solvent surrounding the solute is treated quantum mechanically and the remaining bulk solvent is approximated as a dielectric continuum medium.[120] Obviously, the more solvent molecules treated quantum mechanically, the better the calculated results. The improvement due to increasing the number of solvent molecules in the supermolecular portion including the solute will systematically approach zero in the limit of large n. On the basis of the hybrid supermolecule-continuum approach, the hydration free energy of a solvated electron in water is the free energy of reaction 1, $\Delta G_{hyd}[e^-,n]$ converged to $n \rightarrow \infty$:

$$e^-(gas) + (H_2O)_n(aq) \rightarrow e^-(H_2O)_n(aq) \quad (1)$$

As in our previous calculations of $\Delta G_{hyd}^{298}(H^+)$ and $\Delta G_{hyd}^{298}(HO^-)$, to calculate the free energy of reaction 1 for predicting $\Delta G_{hyd}^{298}(e^-)$, we need to know the Gibbs free energies of e^-(gas), $(H_2O)_n$(aq), and $e^-(H_2O)_n$(aq). For each of the two aqueous clusters $(H_2O)_n$(aq) and $e^-(H_2O)_n$(aq), its free energy, $G[(H_2O)_n(aq)]$ or $G[e^-(H_2O)_n(aq)]$, can be expressed as a sum of the free energy of the corresponding gas-phase cluster, $(H_2O)_n$(gas) or $e^-(H_2O)_n$(gas), and the bulk solvent shift:

$$G[(H_2O)_n(aq)] = G[(H_2O)_n(gas)] + \Delta G_{sol}[(H_2O)_n] \quad (2)$$

$$G[e^-(H_2O)_n(aq)] = G[e^-(H_2O)_n(gas)] + \Delta G_{sol}[e^-(H_2O)_n] \quad (3)$$

Thus, we can evaluate the hydration free energy of the solvated electron via

$$\Delta G_{hyd}[e^-,n] = \Delta G_{gas}[e^-,n] + \Delta\Delta G_{sol}[e^-,n] \quad (4)$$

where

$$\Delta G_{gas}[e^-,n] = G[e^-(H_2O)_n(gas)] - G[(H_2O)_n(gas)] - G[e^-(gas)] \quad (5)$$

is the contribution of the explicitly included water molecules to the hydration free energy of the solvated electron, and

$$\Delta\Delta G_{sol}[e^-,n] = \Delta G_{sol}[e^-(H_2O)_n] - \Delta G_{sol}[(H_2O)_n] \quad (6)$$

is due to the bulk solvent effects. At $T = 298$ K, $\Delta G_{hyd}[e^-,n]$ is converged to $\Delta G_{hyd}^{298}(e^-)$ when $n \rightarrow \infty$. To determine $\Delta G_{hyd}[e^-,n]$ with high accuracy, both $\Delta G_{gas}[e^-,n]$ and $\Delta\Delta G_{sol}[e^-,n]$ must be calculated at a sufficiently high level of theory.

To calculate $\Delta G_{gas}[e^-,n]$ and $\Delta\Delta G_{sol}[e^-,n]$, we first need to optimize geometries of the appropriate structures at a sufficiently high level of theory. Our previous computational studies[121,122] on $\Delta G_{hyd}^{298}(H^+)$ and $\Delta G_{hyd}^{298}(HO^-)$ showed that geometry optimizations in the gas phase using gradient corrected density functional theory (DFT) with Becke's three-parameter hybrid exchange functional and the Lee−Yang−Parr correlation functional (B3LYP)[133−135] together with the 6-31++G** basis set[136] are adequate. Subsequent energy calculations require good treatments of the correlation energy together with very large basis sets. The free energy changes calculated by using geometries optimized at higher levels (with the second-order Møller−Plesset (MP2) method and/or with larger basis sets) were nearly the same as those calculated by using the geometries optimized at the B3LYP/6-31++G** level.[121] The effects of bulk solvent on the optimized geometries are also negligible,[121] as further verified in the present study (see below). These results suggest that the geometries of $(H_2O)_n$ and $e^-(H_2O)_n$ optimized in the gas phase at the B3LYP/6-31++G** level can be used for the solvation free energy calculations. A very recent computational study[137] of the hydration of the OH radical

suggests that one has to be more careful with the choice of DFT exchange−correlation functional when one wishes to describe weak interactions involved in open shell hydrogen-bonded systems. The authors of that study noted that some component of Hartree−Fock exchange needs to be included in the functional in order to obtain reasonable geometries. To examine the reliability of the current DFT geometry optimizations with the B3LYP functional for the systems involved in the present study, we also optimized geometries of some representative tetrameric clusters at the MP2/6-31++G** level. The geometry optimizations were followed by analytical second-derivative calculations to ensure that the optimized geometries are minima on the potential energy hypersurface (all real frequencies) and to evaluate the thermal and vibrational corrections to the gas-phase Gibbs free energies (at 298 K and 1 atm). We considered $n = 4$, 8, and 12 because the structures and energies of the neutral water clusters with these n values have already been established in our previous studies, and we took the geometries and energies for the neutral clusters from our previous work.[121,122]

The geometries optimized at the B3LYP/6-31++G** level were then used in single-point energy calculations at the second-order Møller−Plesset (MP2) level with different basis sets including the correlation-consistent basis sets, aug-cc-pVXZ with X = D, T, and Q.[138−141] To extrapolate to the frozen core complete basis set (CBS) limit, we used a three-parameter, mixed exponential/Gaussian function of the form:

$$E(x) = E_{CBS} + B \exp[-(x-1)] + C \exp[-(x-1)^2] \quad (7)$$

where $x = 2$, 3, and 4 for aug-cc-pVDZ, aug-cc-pVTZ, and aug-cc-pVQZ, respectively.[140] Additional calculations at the coupled-cluster with single and double substitutions with a noniterative triples correction [CCSD(T)][142−144] level were also done with the correlation-consistent basis sets when possible as discussed below. We previously showed in our calculations[121] of $\Delta G_{hyd}^{298}(H^+)$ that the corrections due to core−valence interactions and relativistic effects are small and can be neglected. The overall correction to the electronic energy change due to the core−valence correlation and scalar relativistic effects on $\Delta G_{hyd}^{298}(H^+)$ is less than 0.1 kcal/mol.[121]

Finally, we need to evaluate the bulk solvent shift $\Delta\Delta G_{sol}[e^-n,]$ by performing SCRF calculations on the supermolecular solutes $(H_2O)_n$ and $e^-(H_2O)_n$. The reliability of the SCRF calculation results is dependent on the accuracy of the calculated solvent polarization potential (representing the long-range solute−solvent interaction) in addition to the accuracy of the quantum chemical approximation level for predicting the gas-phase results. Within the continuum model of solvation, the exact solvent electrostatic polarization potential corresponding to a given solute electronic wave function is determined by the solution of the requisite Poisson's equation under certain boundary conditions.[123,145] The full solvent electrostatic polarization consists of both surface and volume polarization.[123] The latter is due to the part of the solute electron charge which quantum mechanically penetrates outside the cavity accommodating the solute. A surface and volume polarization for electrostatic interaction (SVPE) procedure[123−126] has recently been developed to fully evaluate both the surface and volume polarization, and this procedure is also known as the fully polarizable continuum model (FPCM).[146−150] This SVPE procedure, implemented in a local version of the *GAMESS* program,[151] directly determines the volume polarization for an irregularly shaped solute cavity in addition to the more commonly treated surface polarization. In other SCRF implementations, volume polarization effects are ignored or approximately modeled by modifying the surface polarization charge distribution through a simulation and/or charge renormalization,[145,152−158] or the solute charge distribution is simply represented by a set of point charges at the solute nuclei.[159,160] The current version of the SVPE implementation has its own limitations. In particular, the analytic energy derivatives required for geometry optimization have not yet been derived and dynamic solvation effects on vertical electronic excitation energies are not included. Because each method has its own advantages, three different SCRF methods were used in this study to complement each other.

Because the solute cavity surface is defined as a solute electron charge isodensity contour determined self-consistently during the SVPE iteration process, the SVPE results, converged to the exact solution of Poisson's equation with a given numerical tolerance,[123] depend only on the contour value at a given dielectric constant and on the quantum chemical approach that has been used. A single parameter value of 0.001 au has been determined on the basis of an extensive calibration study[124] using the experimental conformational free energy differences (62 experimental observations) of various polar solutes in various solvents. On the basis of the fitting process employed in the calibration, the root-mean-square (rms) deviation of the 62 experimental values from the results calculated by the SVPE method using the 0.001 au contour is 0.096 kcal/mol.[124] The SVPE procedure using the 0.001 au contour has been shown to be reliable for evaluating the bulk solvent effects.[120−122,124] It has also been shown[120,121,124,126] that the solvent shifts determined by SVPE calculations are rather insensitive to the electron correlation level and basis set used, and it is sufficient to perform the SVPE calculations at the MP2/6-31++G** level as done for the calculation of the free energies of solvation of the hydroxide anion and other ions.[121,122] Therefore, we evaluated $\Delta\Delta G_{sol}[e^-,n]$ by using the SVPE procedure at the MP2/6-31++G** level. The other SCRF methods that we used are the integral equation formalism for the polarizable continuum model (IEFPCM)[156,157,161−163] and the quantum Onsager model implemented in the *Gaussian 98* program.[164] It has recently been shown[156] through a comparison with Chipman's work[158] on the surface simulation of volume polarization effects that the IEFPCM formulation actually includes a reasonable surface simulation of volume polarization effects when the charge renormalization scheme is ignored. The solute cavity used in the IEFPCM method is defined as interlocked van der Waals spheres centered at solute nuclei. The default standard parameters associated with the united atom topological model (UATM)[154] in the *Gaussian 98* were used in our IEFPCM calculations. The quantum Onsager model is based on a spherical cavity, whose radius was determined by following the standard procedure[165] of taking the largest distance between the center of mass and the most distant atom plus the van der Waals radius of the atom. The quantum Onsager model was used to qualitatively examine the bulk solvent effects on representative geometries when the geometry optimizations using the IEFPCM method failed to converge. We used a value of 78.5 for the dielectric constant of water.

The vertical electron excitation energies of the most stable structures in water were estimated by using both the single-excitation configuration interaction (CIS) method[166] on the basis of a Hartree−Fock (HF) reference function and time-dependent DFT (TD-DFT) method[167] using the B3LYP functional. For $e^-(H_2O)_4$ and $e^-(H_2O)_8$, we also carried out CAS(n,m)-MP2 calculations, i.e., a complete active space multiconfiguration self-consistent field (CASSCF) calculation including n elec-

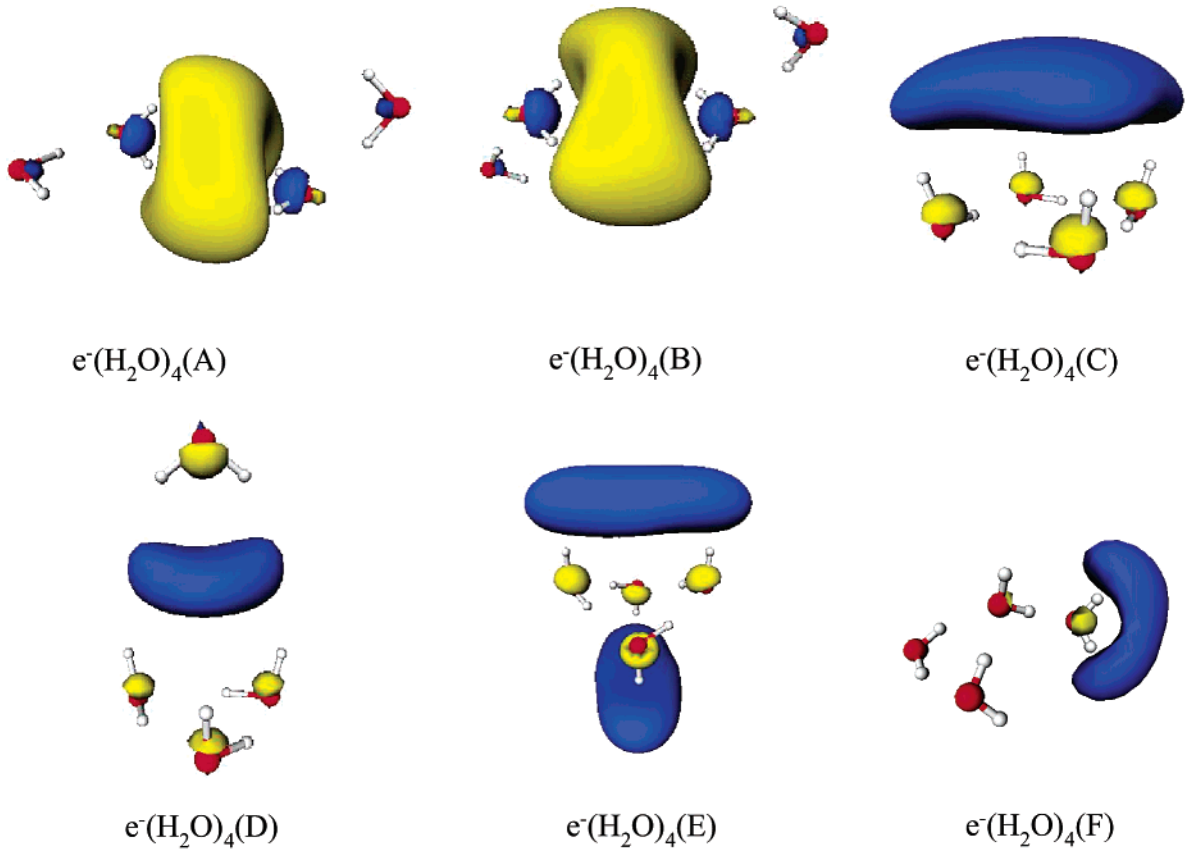

Figure 1. Optimized $e^-(H_2O)_4$ geometries **A**−**F** and the corresponding plots of the singly occupied molecular orbitals (SOMOs) characterizing the solvated electron.

trons occupying *m* molecular orbitals in the active space followed by second-order Møller−Plesset (MP2) perturbation on the multiconfigurational reference state.[168] The basis sets used for calculating the excitation energies include aug-cc-pVDZ, aug-cc-pVTZ, cc-pVDZ, and cc-pVTZ, each augmented by atom-centered Rydberg functions (1s1p1d)[169] on all oxygen atoms. For convenience, these augmented basis sets are denoted by aug-cc-pVDZ+Ryd(O), aug-cc-pVTZ+Ryd(O), cc-pVDZ+Ryd(O), and cc-pVTZ+Ryd(O), respectively. The bulk solvent shifts of the vertical excitation energies were estimated from CIS calculations in the presence of the solvent polarization potential determined by the SVPE calculations for the ground state. The approach for importing the SVPE solvent polarization potential to the CIS calculation is similar to what we previously described for importing the SVPE solvent polarization potential to the GIAO magnetic shielding calculation.[125] This approach is expected to slightly overestimate the bulk solvent shifts of the vertical excitation energies, because it neglects the relaxation of the fast part of the solvent response (due to solvent electrons) to the solute electronic excitation.[145] The slow part of the solvent response (due to solvent nuclei) dominates the solvent polarization.[170]

The geometry optimizations, CIS, TD-DFT, and CAS(*n*,*m*)-MP2 calculations were performed by using the *Gaussian 98* program,[164] and the SVPE solvation calculations were performed by using a local version[123] of the *GAMESS* program.[151] The open-shell CCSD(T) calculations were performed at the R/UCCSD(T) level, where a restricted open shell Hartree−Fock (ROHF) calculation was initially performed and the spin constraint was relaxed in the coupled cluster calculation,[171−173] by using the *MOLPRO* program[174] on a 16-processor SGI Origin 2000 computer. The other MP2 energy calculations were performed by using the *NWChem* program[175] on a 512-processor IBM SP massively parallel supercomputer.

Results and Discussion

The Structure and Chemical Bonding of $e^-(H_2O)_4$. We optimized the $e^-(H_2O)_4$ geometries starting from a variety of potential structures of $e^-(H_2O)_4$ clusters representing either the hydrogen-bonded water cluster with an excess electron corresponding to the cavity model or the $(OH^-\cdots H_3O)(H_2O)_2$ structure proposed by Hameka, Robinson, and Marsden.[29−31] Some of the initial structures were constructed in light of previously reported ab initio studies of gas-phase water cluster anions.[96,99,100] Our DFT-optimized stable geometries are shown in Figure 1 together with the corresponding plots of the singly occupied molecular orbitals (SOMOs) characterizing the solvated electron. The SOMO plots are shown to provide a qualitative picture of the location of the excess electron and are not meant to be quantitative so their spatial extent should not be compared. Their relative energies are summarized in Table 1.

We compared the MP2 energies of the geometries of $e^-(H_2O)_4$(**A**) and $e^-(H_2O)_4$(**C**) optimized at the MP2/6-31++G** level with the corresponding MP2 energies for the geometries at the B3LYP/6-31++G** level and found no significant difference. The total energy of $e^-(H_2O)_4$(**A**) calculated at the MP2/6-31++G**//MP2/6-31++G** level is ∼0.23 kcal/mol lower than that calculated at the MP2/6-31++G**//B3LYP/6-31++G** level. The total energy of $e^-(H_2O)_4$(**C**) calculated at the MP2/6-31++G**//MP2/6-31++G** level is ∼0.19 kcal/mol lower than that calculated at the MP2/6-31++G**//B3LYP/6-31++G** level. The total energy of the most stable neutral $(H_2O)_4$ structure[121] calculated at the MP2/

TABLE 1: Calculated Relative Gibbs Free Energies (kcal/mol) of $e^-(H_2O)_4$ Structures in the Gas Phase (ΔG_{gas}) and Solution (ΔG_{aq}) with $P = 1$ atm

	$e^-(H_2O)_4$					
calculation	**A**[a]	**B**	**C**	**D**	**E**	**F**
relative ΔG_{gas} at 0 K						
MP2/aug-cc-pVDZ	0	−0.01	−0.5	1.0	2.2	−1.0
MP2/aug-cc-pVTZ	0	−0.03	−1.4	0.8	0.7	−1.5
MP2/aug-cc-pVQZ	0	−0.05	−2.0			−1.7
MP2/CBS	0	−0.05	−2.2			−1.8
CCSD(T)/aug-cc-pVDZ	0	−0.00	−1.0			−1.2
best estimate[b]	0	−0.05	−2.5			−2.0
relative ΔG_{gas} shift (0 K → 298 K)	0	0.8	6.4	2.1	6.0	3.6
estimated relative ΔG_{gas} at 298 K	0	0.7	3.9	∼3	∼7	1.6
relative bulk solvent shift (SVPE)	0	−0.1	3.6	0.7	2.5	−1.2
estimated relative ΔG_{aq} at 298 K	0	0.6	7.5	∼4	∼9	0.4

[a] The letters **A**−**F** respectively refer to the structures $e^-(H_2O)_4$(**A**)−$e^-(H_2O)_4$(**F**) shown in Figure 1. [b] The best estimate is the MP2/CBS value plus the higher order electron correlation correction estimated as the energy shift from the MP2/aug-cc-pVDZ value to the corresponding CCSD(T)/aug-cc-pVDZ value.

6-31++G**//MP2/6-31++G** level is ∼0.21 kcal/mol lower than that calculated at the MP2/6-31++G**//B3LYP/6-31++G** level. Thus, the net changes of the hydration energies would be only ∼0.02 and −0.02 kcal/mol for structures **A** and **C**, respectively, when the MP2/6-31++G**//B3LYP/6-31++G** energies are all replaced by the corresponding MP2/6-31++G**//MP2/6-31++G** energies.

Structures $e^-(H_2O)_4$(**C**), $e^-(H_2O)_4$(**E**), and $e^-(H_2O)_4$(**F**) are all associated with four O···HO hydrogen bonds as found for the most stable, cycle $(H_2O)_4$ cluster structure. The excess electron can be regarded as being dipole-bound in some of these structures.[98,100] The structure $e^-(H_2O)_4$(**D**) has only three O···HO hydrogen bonds on the three-water ring, and the excess electron is solvated internally between the three-water ring and the other water molecule. The $e^-(H_2O)_4$(**A**) and $e^-(H_2O)_4$(**B**) structures have only two O···HO hydrogen bonds each, and the excess electron is internally solvated between two hydrogen-bonded water dimers. The only structural difference between $e^-(H_2O)_4$(**A**) and $e^-(H_2O)_4$(**B**) is the relative orientation of the two water molecules which are closest to the excess electron at the molecular center; these two water molecules are nearly in the same plane in $e^-(H_2O)_4$(**B**), whereas the two planes representing these two water molecules are nearly perpendicular to each other in $e^-(H_2O)_4$(**A**). The structure $e^-(H_2O)_4$(**B**) was first found by Tsurusawa and Iwata.[100] Kim et al.[99] studied structures $e^-(H_2O)_4$(**C**) and $e^-(H_2O)_4$(**E**) and other higher-energy structures and concluded that the structure $e^-(H_2O)_4$(**B**) is the most stable tetramer in the gas phase. The structures $e^-(H_2O)_4$(**A**), $e^-(H_2O)_4$(**D**), and $e^-(H_2O)_4$(**F**) are reported here for the first time.

The electronic stability of the gas-phase cluster structures is related to their vertical electron detachment energies (VDEs). Very high-level ab initio calculations are required to accurately predict this property. For example, previous studies[176−179] on VDEs of a variety of anionic clusters indicate that, whereas the CCSD(T) and QCISD(T) methods can predict the VDEs with a high accuracy, the MP2 method considerably underestimates the VDEs. Nevertheless, in the present study, we only require the qualitative VDE value for a given cluster structure in order to determine whether the cluster structure has a bound electron at that geometry. DFT calculations using the B3LYP functional can be used to predict VDEs semiquantitatively; in addition, the DFT results are less sensitive to the size of the basis set.[180,181]

TABLE 2: Calculated Vertical Electron Detachment Energy (VDE, in eV) of the $e^-(H_2O)_n$ ($n = 4$, 8, and 12) Clusters in the Gas Phase Compared with Available Experimental Data

	$e^-(H_2O)_4$					
method	**A**	**B**	**C**	**D**	**E**	**F**
B3LYP/6-31++G**	0.77	0.78	0.09	0.53	−0.15	0.39
MP2/aug-cc-pVDZ+diff(2sp,s)[a]	0.40	0.41	0.08			
MP2/aug-cc-pVDZ	0.35	0.36	−0.23	−0.23		
MP2/aug-cc-pVTZ	0.39	0.40	−0.14	−0.14		
MP2/aug-cc-pVQZ	0.41	0.42	−0.10	−0.10		
MP2/CBS	0.41	0.42	−0.08	−0.08		
CCSD(T)/aug-cc-pVDZ	0.39	0.40	−0.17	−0.17		
best estimate[c]	0.45	0.46	−0.02	−0.02		

	$e^-(H_2O)_8$					$e^-(H_2O)_{12}$	
method	**A**	**B**	**C**	**D**	**E**	**A**	**B**
B3LYP/6-31++G**	1.41	0.44	0.63	0.52	0.97	1.90	1.03
MP2/aug-cc-pVDZ+diff(2sp,s)[a]	0.92	0.26					
exptl[b]		0.32	0.53				

[a] aug-cc-pVDZ+diff(2sp,s) refers to the aug-cc-pVDZ basis set augmented by additional sets of diffuse functions for oxygen (2sp) and hydrogen (s) atoms, as used in ref 101. [b] Experimental VDE values from ref 117. [c] The best estimate is the MP2/CBS value plus the higher order electron correlation correction estimated as the change from the MP2/aug-cc-pVDZ value to the corresponding CCSD(T)/aug-cc-pVDZ value.

Our calculated VDE values for $e^-(H_2O)_4$ are summarized in Table 2, together with those for $e^-(H_2O)_8$ and $e^-(H_2O)_{12}$. As shown in Table 2, the VDE values calculated at the B3LYP/6-31++G** level are systematically higher than the corresponding values at the MP2 level. The VDE values calculated at the CCSD(T)/aug-cc-pVDZ level are slightly larger than the corresponding values at the MP2/aug-cc-pVDZ level and closer to the corresponding B3LYP/6-31++G** values. The differences between the best estimates and the corresponding B3LYP/6-31++G** values suggest that the B3LYP/6-31++G** calculations likely overestimate the VDE values for these structures. The accuracy of the calculated VDE values can also be assessed by a comparison with available experimental data for $e^-(H_2O)_8$ (see below). The data for $e^-(H_2O)_4$ clearly suggest that structures $e^-(H_2O)_4$(**A**), $e^-(H_2O)_4$(**B**), $e^-(H_2O)_4$(**D**), and $e^-(H_2O)_4$(**F**) are electron-bound, whereas the excess electron in $e^-(H_2O)_4$(**E**) is not bound in the gas phase. The unbound gas-phase $e^-(H_2O)_4$(**E**) structure is an artifact of the theoretical calculation in which the excess electron is forced to occupy a SOMO that is not of infinite size. For $e^-(H_2O)_4$(**C**), the very small positive VDE value calculated at the B3LYP/6-31++G** level and the best estimate which yields a very small negative VDE value (i.e., the MP2/CBS value plus the shift from the MP2/aug-cc-pVDZ to the CCSD(T)/aug-cc-pVDZ) suggest that the excess electron is either very weakly bound or unbound in $e^-(H_2O)_4$(**C**).

The vertical electron detachment energies of the $e^-(H_2O)_4$ structures discussed above could differ considerably from the corresponding adiabatic detachment energies because these structures will become very unstable after the excess electron is removed. Considerable geometry relaxation/change occurs on geometry optimization of the neutral species starting from the corresponding anionic geometry. The geometry optimizations of the neutral species starting from the $e^-(H_2O)_4$ structures all optimize to the previously optimized most stable four-water ring structure,[121,122] except for that from the $e^-(H_2O)_4$(**B**) structure. The geometry optimization starting from the $e^-(H_2O)_4$(**B**) structure leads to a four-water ring structure of $(H_2O)_4$ which

differs from the most stable $(H_2O)_4$ structure only in the relative orientations of the four O−H bonds which are not involved in a hydrogen bond. The energy of this new $(H_2O)_4$ structure is ∼1.2 kcal/mol higher that the most stable $(H_2O)_4$ structure.[121,122]

In addition to the geometries in Figure 1, we also tried to obtain other possible stable geometries by using different initial structures. All of the optimizations eventually went to either the geometries shown in Figure 1 or to higher energy structures associated with saddle points on the potential energy surface. For example, we tested an initial structure with four water molecules tetrahedrally coordinating to the electron at the mass center through one of the two hydrogen atoms for each water molecule. During the optimization process without symmetry constraints, the geometry slowly distorted and finally went to structure $e^-(H_2O)_4$(**A**) (with C_2 symmetry). Starting from a similar initial structure with fixed S_4 point-group symmetry led to a higher energy second-order saddle point.

On the basis of Hameka, Robinson, and Marsden's structural model,[29] our initial geometry for the candidate $(OH^-\cdots H_3O)(H_2O)_2$ structure was constructed by using our previously optimized geometry[120] of $HO^-(H_2O)_3$ with an additional H atom attached to one of the water molecules. The initial $(OH^-\cdots H_3O)(H_2O)_2$ structure thus consists of a neutral hydronium (H_3O) radical, a hydroxide anion (HO^-), and two neutral water (H_2O) molecules; the hydroxide oxygen has a hydrogen bond with each of the other three species. However, during the geometry optimization procedure, the hydrogen atom of H_3O directly hydrogen-bonding to the hydroxide oxygen was gradually transferred to the hydroxide oxygen along the hydrogen bond. The finally converged geometry is $e^-(H_2O)_4$(**F**) in Figure 1, a hydrogen-bonded four-water cluster with an excess electron. This means that the candidate $(OH^-\cdots H_3O)(H_2O)_2$ structure is not stable in the gas phase. We tested the geometry optimization by using the IEFPCM method at the B3LYP/6-31++G** level in order to examine whether the candidate $(OH^-\cdots H_3O)(H_2O)_2$ structure can be stabilized by bulk solvent effects or not. The geometry optimization in solution led to qualitatively the same results as obtained from the corresponding gas-phase geometry optimization. The hydrogen was clearly transferred from the H_3O radical to the hydroxide oxygen, and the final geometry is nearly identical to the $e^-(H_2O)_4$(**F**) geometry optimized in the gas phase, although the default convergence criterion of the geometry optimization could not be achieved due to the relatively low accuracy of the energy gradient calculations in the IEFPCM method. Our results clearly show that the $(OH^-\cdots H_3O)(H_2O)_2$-type complex is not a stable structure in either the gas phase or solution.

The energetic results listed in Table 1 reveal that structure $e^-(H_2O)_4$(**C**) indeed has the lowest gas-phase energy ΔE (including the zero-point vibrational energy correction), as predicted by Kim et al.[99] After accounting for the effects of thermal motion at 298 K, the Gibbs free energy of $e^-(H_2O)_4$(**C**) becomes higher than the Gibbs free energies of $e^-(H_2O)_4$(**A**), $e^-(H_2O)_4$(**B**), $e^-(H_2O)_4$(**D**), and $e^-(H_2O)_4$(**F**); the lowest Gibbs free energy at 298 K is now associated with our new structure $e^-(H_2O)_4$(**A**). This is analogous to Gutowski et al.'s finding[182] that the relative stability of different $(HF)_n^-$ cluster structures at 298 K is different from that at 0 K. They suggested that the vibrational contribution to the entropy favors less rigid solvated electron structures over more rigid, hydrogen-bonded, dipole-bound structures.[182] The bulk solvent effects also differentially stabilize the different tetramer clusters. The lowest Gibbs free energy is still associated with $e^-(H_2O)_4$(**A**) in solution, even though it only has two O···HO hydrogen bonds.

TABLE 3: Dipole Moments (μ, in Debye) of $(H_2O)_n$ at the $e^-(H_2O)_n$ Geometries (n = 4, 8, and 12) and the $(H_2O)_n$ Cluster Reorganization Energies (in kcal/mol) Calculated at the B3LYP/6-31++G Level in the Gas Phase**

	$e^-(H_2O)_4$					
property	**A**	**B**	**C**	**D**	**E**	**F**
μ of $(H_2O)_n$ at the $e^-(H_2O)_n$ geometry	1.95	0.14	5.88	2.34	0.00	9.09
reorganization energy[a] of $(H_2O)_n$	26.2	26.3	7.6	21.4	4.0	15.9

	$e^-(H_2O)_8$					$e^-(H_2O)_{12}$	
property	**A**	**B**	**C**	**D**	**E**	**A**	**B**
μ of $(H_2O)_n$ at the $e^-(H_2O)_n$ geometry	14.05	10.92	13.21	13.14	0.00	22.30	21.21
reorganization energy[a] of $(H_2O)_n$	38.3	11.0	15.6	15.6	32.6	43.9	21.3

[a] The reorganization energy was calculated as the energy change of $(H_2O)_n$ from the $e^-(H_2O)_n$ geometry to the optimized most stable geometry of $(H_2O)_n$.

It is well established that molecules with a dipole moment greater than ∼1.625 D can bind an electron.[183] Previous computational studies examined the possible correlation[98,101,184] between the relative stability of the $e^-(H_2O)_n$ structures and the dipole moments of the corresponding neutral species at the optimum anion geometries. The dipole moments of the neutral terameric clusters taken from the anion geometries (Table 3) show that the clusters with the largest dipole moments, **C** (5.88 D) and **F** (9.09 D), have the largest gas-phase binding energy at 0 K. However, the lowest energy is associated with structure **C** with the second largest dipole moment, rather than structure **F** with the largest dipole moment. The calculated nonzero components of the quadrupole moments (D-Å), −30.15 (*XX*), −30.15 (*YY*), and −23.10 (*ZZ*) for structure **C** and −26.14 (*XX*), −29.49 (*YY*), −25.00 (*ZZ*), −0.82 (*XY*), −2.01 (*XZ*), and −6.84 (*YZ*) for structure **F**, do not differ enough to explain why the $e^-(H_2O)_4$(**C**) structure is more stable than the $e^-(H_2O)_4$(**F**) structure at 0 K in the gas phase. This suggests that other nonelectrostatic interactions can also affect the relative stability of these structures in the gas phase and, as discussed below, significantly in solution.

The thermodynamic stability of the $e^-(H_2O)_4$(**A**) structure can be attributed, in part, to the contribution from a rarely recognized type of bond, which we define as the electron-hydrogen or e⁻···HO bond, between the excess electron and water hydrogen. A graphic representation of the two strong e⁻···HO bonds existing in structure $e^-(H_2O)_4$(**A**) is given in Figure 2. Tsurusawa and Iwata first proposed the concept of such a chemical bond, which was denoted by {e}HO, in their recent computational studies of gas-phase water clusters with an excess electron.[98,100,185−187] Our results listed in Table 1 further indicate that the strength of an e⁻···HO bond should be comparable to that of an O···HO hydrogen bond, 5.0 kcal/mol in $(H_2O)_2$.[188,189] Because the excess electron is clearly centered at the molecular center of the $e^-(H_2O)_4$(**A**) and $e^-(H_2O)_4$(**B**) structures, we can determine the e⁻···H distance and e⁻···HO bond angles on the basis of the optimized geometries. The $e^-(H_2O)_4$(**B**) structure has four equivalently weak and bent e⁻···HO bonds with an e⁻···H distance of ∼1.85 Å and an e⁻···HO bond angle of ∼104°. The $e^-(H_2O)_4$(**A**) structure mainly has two equivalent, stronger e⁻···HO bonds with a shorter e⁻···H distance of ∼1.70 Å and a larger e⁻···HO bond angle of ∼123°; the other two equivalent, longer and bent e⁻···HO bonds are weaker with an e⁻···H distance of ∼1.91 Å and an e⁻···HO bond angle of ∼105°. For the other structures, although we could not simply

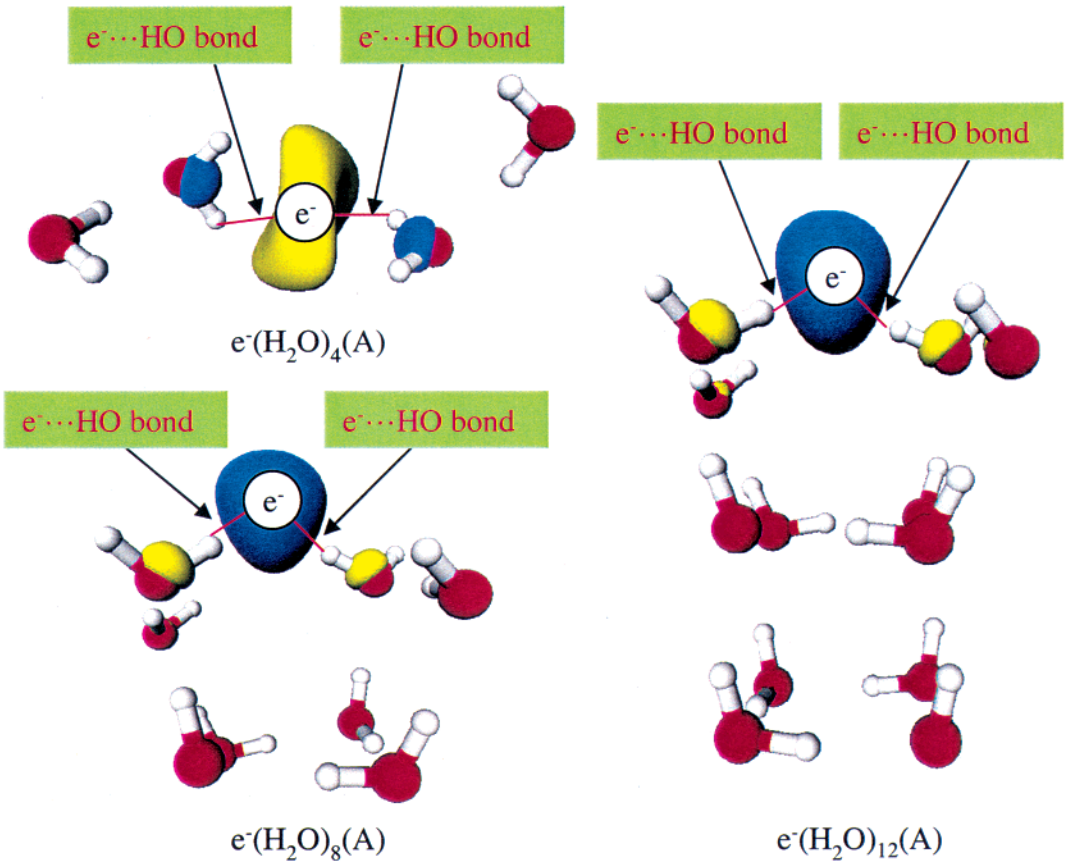

Figure 2. Graphical representation of the $e^-\cdots$HO bonds in the most stable structures, $e^-(H_2O)_4$(**A**), $e^-(H_2O)_8$(**A**), and $e^-(H_2O)_{12}$(**A**), in water.

assign the exact position of the center of the excess electron, Figure 1 clearly suggests that the $e^-(H_2O)_4$(**D**) structure has a total of five weak $e^-\cdots$HO bonds. In addition, it is possible to describe the $e^-(H_2O)_4$(**C**) and $e^-(H_2O)_4$(**F**) structures as being associated with $e^-\cdots$HO bonds. We note that similar gas-phase water clusters are usually described as being dipole-bound.[100] However, the $e^-\cdots$HO bonds in these dipole-bound clusters should be much weaker than those in the structures with the electron solvated internally. Our energetic results in Table 1 suggest that the thermal motion favorably stabilizes $e^-\cdots$HO bonds containing structures in general and that the most stable structure at room temperature has a tendency to have a SOMO shape like an s orbital as much as possible so as to form stronger $e^-\cdots$HO bonds. We also compared the SOMO shapes determined by the gas-phase calculations with those from the corresponding single-point calculations accounting for the bulk solvent effects, and found no significant differences. There is also a tendency to have fewer and stronger $e^-\cdots$HO bonds, rather than more and weaker $e^-\cdots$HO bonds. This model provides a qualitative explanation as to why $e^-(H_2O)_4$(**A**) is the most stable structure at 298 K.

To gain more insight into the role of the $e^-\cdots$HO bonds, we calculated the reorganization energy of the $(H_2O)_n$ cluster needed to place the excess electron into the $(H_2O)_n$ structure The reorganization energies given in Table 3 were calculated as the difference in the energy of the $(H_2O)_n$ clusters taken from the $e^-(H_2O)_n$ geometries from that of the optimized most stable geometries of $(H_2O)_n$. The data in Table 3 show that the largest reorganization energies, ~26 kcal/mol, of $e^-(H_2O)_4$ are associated with the most stable structures in solution, i.e., the structures with the strongest $e^-\cdots$HO bonds [$e^-(H_2O)_4$(**A**) and $e^-(H_2O)_4$(**B**)]. After the excess electron in $e^-(H_2O)_4$(**A**) or $e^-(H_2O)_4$(**B**) is removed, the strong $e^-\cdots$HO bonds no longer exist and the neutral cluster has only two O···HO hydrogen bonds in contrast to four O···HO hydrogen bonds in the most stable $(H_2O)_4$ structure. Structure $e^-(H_2O)_4$(**D**), with the next largest reorganization energy, ~21 kcal/mol, has more, but weaker, $e^-\cdots$HO bonds. The corresponding $(H_2O)_4$ cluster at the $e^-(H_2O)_4$(**D**) geometry has three O···HO hydrogen bonds as compared to four O···HO hydrogen bonds in the most stable $(H_2O)_4$ structure. Structure $e^-(H_2O)_4$(**F**) with four O···HO hydrogen bonds has the next largest reorganization energy and the remaining two structures, $e^-(H_2O)_4$(**C**) and $e^-(H_2O)_4$(**E**), each with four O···HO hydrogen bonds, have the lowest reorganization energies. Clearly, the energy needed to distort the structure to accommodate the excess electron does not play the dominant role in determining the most stable structure in solution.

We note that all of the energy calculations discussed above are based on the geometries optimized in the gas phase. To examine whether the bulk solvent effects on the $e^-(H_2O)_4$ geometries could qualitatively change the relative stability of different $e^-(H_2O)_4$ structures, we tried to refine the geometries of two representative structures, i.e., $e^-(H_2O)_4$(**A**) and $e^-(H_2O)_4$(**C**), in solution by using the IEFPCM method. Because none of the geometry optimizations with the IEFPCM would converge on the basis of the default convergence criterions, we had to use the quantum Onsager model for the geometry optimizations in order to obtain converged results. The geometries of $e^-(H_2O)_4$(**A**) and $e^-(H_2O)_4$(**C**) optimized in solution at the same level (B3LYP/6-31++G**) are nearly identical to the corresponding geometries optimized in the gas phase; the total free energy changes from the gas-phase geometries to the corresponding solution geometries are all smaller than 0.1 kcal/

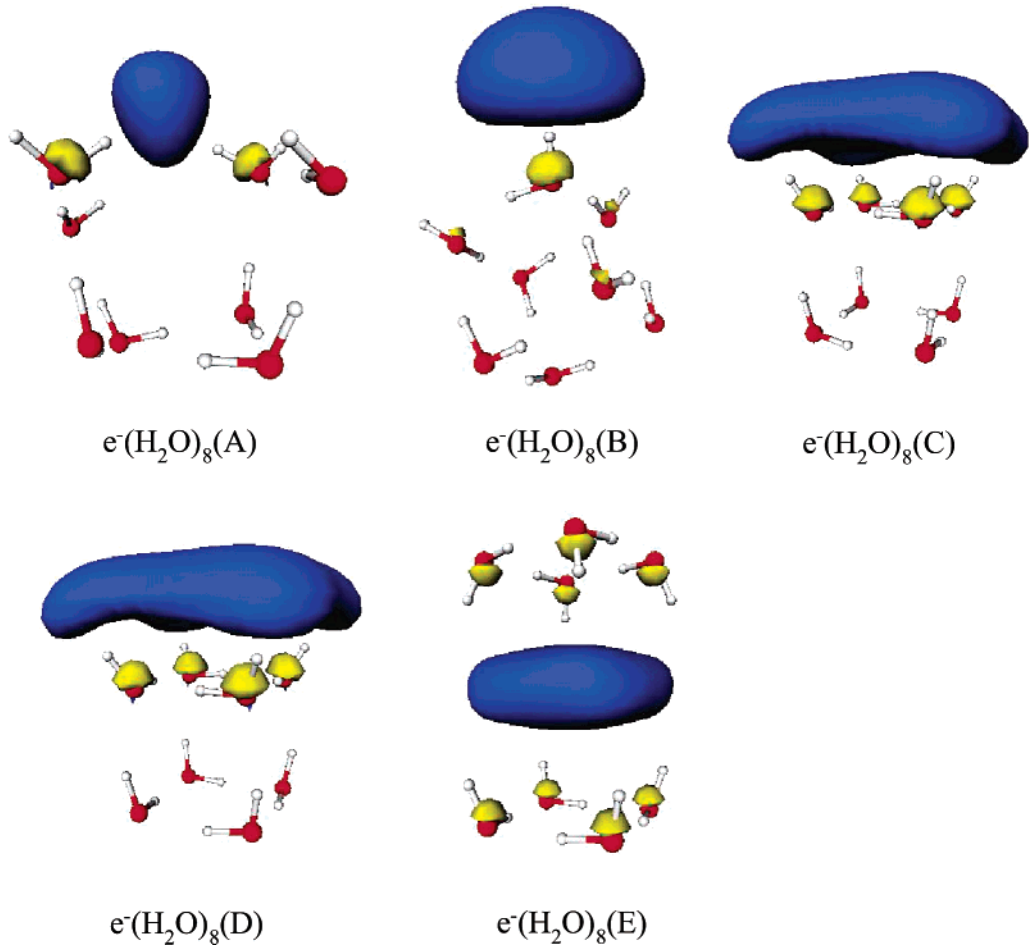

Figure 3. Optimized $e^-(H_2O)_8$ geometries **A**−**E** and the corresponding plots of the singly occupied molecular orbitals (SOMOs) characterizing the solvated electron.

mol. Thus we ignored the bulk solvent effects on other $e^-(H_2O)_n$ geometries and simply used the gas-phase geometries for our final energy calculations.

The Structure and Chemical Bonding of $e^-(H_2O)_8$. Five optimized geometries of $e^-(H_2O)_8$ are depicted in Figure 3, together with the corresponding plots of the SOMOs. During our work on these structures, Lee and Kim[101] reported three gas-phase $e^-(H_2O)_8$ cluster structures that are the same as our $e^-(H_2O)_8$(**B**), $e^-(H_2O)_8$(**C**), and $e^-(H_2O)_8$(**D**) structures, and concluded that $e^-(H_2O)_8$(**B**) is the most stable structure. The $e^-(H_2O)_8$(**B**), $e^-(H_2O)_8$(**C**), and $e^-(H_2O)_8$(**D**) structures each have 12 O···HO hydrogen bonds. On the basis of our simple model for the e⁻···H−O bond, $e^-(H_2O)_8$(**B**) has a "perfect" e⁻···HO bond angle of ∼180°. Both $e^-(H_2O)_8$(**C**) and $e^-(H_2O)_8$(**D**) are associated with weak e⁻···HO bonds as found for $e^-(H_2O)_4$(**C**). The $e^-(H_2O)_8$(**A**) and $e^-(H_2O)_8$(**E**) structures with the electron solvated internally or semi-internally are reported here for the first time. $e^-(H_2O)_8$(**A**) has 10 O···HO hydrogen bonds and two equivalent strong e⁻···HO bonds (Figure 2), whereas $e^-(H_2O)_8$(**E**) has eight O···HO hydrogen bonds and eight equivalent weak e⁻···HO bonds.

As shown in Table 2, the calculated VDE values for the five $e^-(H_2O)_8$ structures are all positive, indicating that these structures are all electron-bound. The gas-phase $e^-(H_2O)_8$ cluster was observed by Kim et al.[117] by using photoelectron spectroscopy. The photoelectron spectrum of $e^-(H_2O)_8$ cluster shows a strong peak at 0.32 eV and a relatively weaker peak at 0.53 eV. Our calculated relative energies at 0 K listed in Table 4 and VDE values in Table 2 are in good agreement with the

TABLE 4: Calculated Relative Gibbs Free Energies (kcal/mol) of $e^-(H_2O)_8$ Structures in the Gas Phase (ΔG_{gas}) and Solution (ΔG_{aq}) when $P = 1$ atm

	$e^-(H_2O)_8$				
calculation	**A**[a]	**B**	**C**	**D**	**E**
relative ΔG_{gas} at 0 K					
MP2/aug-cc-pVDZ	0	−3.5	−3.0	−2.8	6.6
MP2/aug-cc-pVTZ	0	−4.5	−3.9	−3.7	5.8
MP2/aug-cc-pVQZ	0	−4.6			5.4
MP2/CBS	0	−4.7			5.2
relative ΔG_{gas} shift (0 K → 298 K)	0	2.3	2.8	2.8	−0.5
estimated relative ΔG_{gas} at 298 K	0	−2.4	∼ −1	∼ −1	4.7
relative bulk solvent shift (SVPE)	0		10.0	10.0	2.6
estimated relative ΔG_{aq} at 298 K	0		∼9	∼9	7.3
relative bulk solvent shift (IEFPCM)	0	5.9	7.7	7.8	
estimated relative ΔG_{aq} at 298 K	0	3.5	∼7	∼7	

[a] The letters **A**−**E** respectively refer to the structures $e^-(H_2O)_8$(**A**)−$e^-(H_2O)_8$(**E**) shown in Figure 2.

experimental spectra. In agreement with Lee and Kim's conclusion,[101] our results in Table 4 indicate that the $e^-(H_2O)_8$(**B**) structure has the lowest energy at 0 K in the gas phase; it also has the lowest Gibbs free energy at 298 K in the gas phase. The next most stable structures at 0 K are $e^-(H_2O)_8$(**C**) and $e^-(H_2O)_8$(**D**) with nearly identical relative energies; the difference between $e^-(H_2O)_8$(**C**) and $e^-(H_2O)_8$(**D**) is ∼0.2 kcal/mol. These results suggest that the strong peak observed in the photoelectron spectrum is associated with the electron ionization from $e^-(H_2O)_8$(**B**), whereas the weaker peak corresponds to the electron ionization from both $e^-(H_2O)_8$(**C**) and $e^-(H_2O)_8$(**D**),

consistent with Lee and Kim's conclusions.[101] On the basis of this assignment, the VDE values calculated at the B3LYP/6-31++G** level are systematically larger than the corresponding experimental data by ~0.1 eV, whereas the VDE value calculated for $e^-(H_2O)_8$(**B**) at the MP2/aug-cc-pVDZ+diff(2sp,s) level is smaller than the experimental value by ~0.1 eV. In addition, our VDE value of 0.26 eV calculated for $e^-(H_2O)_8$(**B**) at the MP2/aug-cc-pVDZ+diff(2sp,s) level using the geometry optimized at the B3LYP/6-31++G** level is in excellent agreement with the VDE value of 0.25 eV calculated by Lee and Kim[101] at the same level but using the geometry optimized at the B3LYP/6-311++G**+diff(sp) level, again showing that the DFT geometries are not particularly sensitive to the basis set if a large enough basis set is used.

The dipole moments of the neutral species listed in Table 3 show that the lowest energy at 0 K is associated with the $e^-(H_2O)_8$(**B**) structure corresponding to the second smallest dipole moment (10.92 D). In addition, there are two more structures with smaller dipole moments that are also lower in energy at 0 K than the structure with the largest dipole moment, $e^-(H_2O)_8$(**A**). The least stable structure at 0 K in the gas phase is associated with the $e^-(H_2O)_8$(**E**) structure with the smallest (0 D) dipole moment. Interestingly, the most stable $e^-(H_2O)_8$(**A**) structure at 298 K in water corresponds to the largest dipole moment (14.05 D). As found for $e^-(H_2O)_4$, the largest reorganization energy, ~38 kcal/mol, of $e^-(H_2O)_8$ is associated with the structure $e^-(H_2O)_8$(**A**), which is the most stable in solution and has two strong $e^-\cdots$HO bonds. The $(H_2O)_8$ cluster at the $e^-(H_2O)_8$(**A**) geometry has 10 O···HO hydrogen bonds as compared to 12 O···HO hydrogen bonds in the most stable $(H_2O)_8$ structure. Structure $e^-(H_2O)_8$(**E**) has the second largest reorganization energy, ~33 kcal/mol, and as in $e^-(H_2O)_4$, this structure has more, but much weaker, $e^-\cdots$HO bonds. The $(H_2O)_8$ cluster at the $e^-(H_2O)_8$(**E**) geometry has only eight O···HO hydrogen bonds as compared to 12 O···HO hydrogen bonds in the most stable $(H_2O)_8$ structure. The other three $(H_2O)_8$ structures associated with $e^-(H_2O)_8$, derived from **B**, **C**, and **D**, all have 12 O···HO hydrogen bonds and have the smallest reorganization energies.

We list in Table 4 the relative bulk solvent shifts calculated by using the SVPE and IEFPCM methods for only four structures each because neither of the currently available implementations of the two methods leads to fully converged SCRF results for some of the unusually irregular cavities corresponding to the supermolecular solute structures. As noted in our original paper[123] for the SVPE method, the three-dimensional integration algorithm used in the present version of the SVPE implementation is based on a single center of the solute cavity defined as the electron isodensity contour. The single-center integration places a mild restriction on the shape of the solute cavity, i.e., it must be possible to find a central origin inside the solute from which any point on the cavity surface can be uniquely identified by its solid angle.[123] Thus, cavities having reentrant surfaces cannot be treated without changing the integration algorithm from the single-center to multiple-center. The $e^-(H_2O)_8$(**B**) structure was found to have a reentrant cavity surface (caused by the e···HO bond) in the SVPE calculation. The IEFPCM implementation in the *Gaussian 98* defines the solute cavity as an interlocked spheres centered at solute nuclei. The IEFPCM implementation was successful in the calculation on $e^-(H_2O)_8$(**B**), although it failed for $e^-(H_2O)_8$(**F**) in which the spheres representing one set of four hydrogen-bonded water molecules do not overlap with the other spheres representing the other set of four water molecules. Nevertheless, the results summarized in Table 4 are sufficient for our purpose of the qualitative comparison of the relative stability of these five structures. Besides the minor difference in the cavity definition, the major difference between the SVPE and IEFPCM methods is related to the treatment of the volume polarization.[126] Whereas the SVPE method directly evaluates the volume polarization effects through a three-dimensional integration algorithm, the IEFPCM method implicitly simulates the volume polarization effects through modifying the surface polarization charge distribution on the two-dimensional cavity surface. Although this difference could lead to significantly different results for other properties,[126] we have already demonstrated that the volume polarization effects on the relative solvation free energies of different isomers of the same molecule are relatively small.[124] This is because the volume polarization effects on the absolute solvation free energies of the different isomers approximately cancel.[124] As shown in Table 4, this expectation is supported by the qualitative agreement between the relative IEFPCM solvent shifts and the relative SVPE solvent shifts for the three $e^-(H_2O)_8$ structures (i.e., **A**, **C**, and **D**) for which both kinds of results have been obtained.

As shown in Table 4, the bulk solvent effects significantly favor the $e^-(H_2O)_8$(**A**) and $e^-(H_2O)_8$(**E**) structures with the electron solvated internally or semiinternally so that $e^-(H_2O)_8$(**A**) is the most stable structure in solution. The free energy of $e^-(H_2O)_8$(**B**) is ~3.5 kcal/mol higher than $e^-(H_2O)_8$(**A**) in solution, indicating that in solution the total strength of 10 O···HO bonds plus two strong $e^-\cdots$HO bonds in $e^-(H_2O)_8$(**A**) is stronger than that of 12 O···HO bonds plus one perfect $e^-\cdots$HO bond in $e^-(H_2O)_8$(**B**). In addition, the relative free energies in solution listed in Table 4 also reveal that, in solution, the total strength of 10 O···HO bonds plus eight weak $e^-\cdots$HO bonds in $e^-(H_2O)_8$(**E**) is stronger than that of 12 O···HO bonds plus four very weak $e^-\cdots$HO bonds in $e^-(H_2O)_8$(**C**) and in $e^-(H_2O)_8$(**D**), but still weaker than that of 10 O···HO bonds plus two strong $e^-\cdots$HO bonds in $e^-(H_2O)_8$(**A**) and than that of 12 O···HO bonds plus one strong $e^-\cdots$HO bond in $e^-(H_2O)_8$(**B**). This suggests that the strengths of different $e^-\cdots$HO bonds can be affected by going from the gas phase to aqueous solution.

The most stable $e^-(H_2O)_8$ structure, $e^-(H_2O)_8$(**A**), in solution can be constructed from adding four water molecules (as a four-water ring) to the most stable $e^-(H_2O)_4$ structure, i.e., $e^-(H_2O)_4$(**A**). In fact, we showed that the $e^-(H_2O)_4$(**A**) structure can be obtained by removing the four-water ring in $e^-(H_2O)_8$(**A**) and then performing a geometry optimization. The structural change from $e^-(H_2O)_4$(**A**) to $e^-(H_2O)_8$(**A**) does not affect the two strong $e^-\cdots$HO bonds, but the other two weaker $e^-\cdots$HO bonds disappear due to formation of the O···HO bonds with the added four-water ring.

The Structure and Chemical Bonding of $e^-(H_2O)_{12}$. Kim et al.[94] studied the relative stability of a total of 12 possible $e^-(H_2O)_{12}$ structures in the gas phase by performing ab initio calculations. In light of the their results, we only optimized two geometries of $e^-(H_2O)_{12}$, i.e., $e^-(H_2O)_{12}$(**A**) and $e^-(H_2O)_{12}$(**B**) in Figure 4. The calculated positive VDE values listed in Table 2 indicate that these two structures are all electron-bound. Kim et al.'s results[94] indicate that a structure like $e^-(H_2O)_{12}$(**A**) has the lowest energy in the gas phase. The structure $e^-(H_2O)_{12}$(**B**) in Figure 4, which consists of three four-water rings, is new, but is similar to the second lowest energy (ΔE_0) structure of Kim et al.'s at 0 K; the difference between our structure and their structure is in the orientation of the four O···HO bonds in the middle ring relative to the other two rings. In agreement

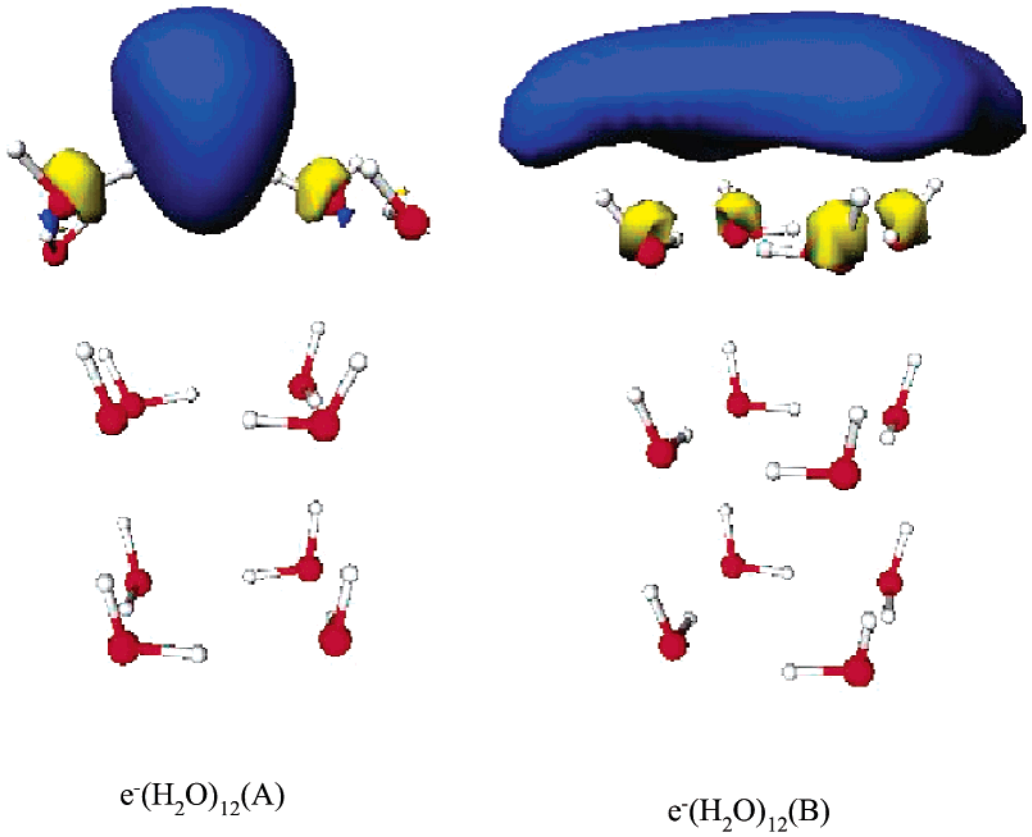

Figure 4. Optimized $e^-(H_2O)_{12}$(**A**) and $e^-(H_2O)_{12}$(**B**) geometries and the corresponding plots of the singly occupied molecular orbitals (SOMOs) characterizing the solvated electron.

with Kim et al.'s results,[94] our calculated energies (with the ZPVE corrections) indicate that $e^-(H_2O)_{12}$(**A**) is more stable than $e^-(H_2O)_{12}$(**B**) by ~1.3 kcal/mol at the MP2/aug-cc-pVDZ level or ~1.4 kcal/mol at the MP2/aug-cc-pVTZ level at 0 K. Both the thermal motion and bulk solvent effects favor the $e^-(H_2O)_{12}$(**A**) structure so that, at 298 K and 1 atm, $e^-(H_2O)_{12}$(**A**) is more stable than $e^-(H_2O)_{12}$(**B**) by ~3.6 kcal/mol in the gas phase and by ~8.2 kcal/mol in the solution.

The calculated (B3LYP/6-31++G**) dipole moment, 22.30 D, of the neutral species corresponding to structure $e^-(H_2O)_{12}$(**A**) is slightly larger than that, 21.21 D, of the neutral species corresponding to structure $e^-(H_2O)_{12}$(**B**). This is qualitatively consistent with the relative stability of structures $e^-(H_2O)_{12}$(**A**) and $e^-(H_2O)_{12}$(**B**) at both 0 and 298 K in both the gas phase and solution. Again, the structure $e^-(H_2O)_{12}$(**A**), with the largest reorganization energy (Table 3), is the most stable in solution and has two strong e⁻···HO bonds.

In terms of the bonding holding the clusters together, the thermodynamic stability of $e^-(H_2O)_{12}$(**A**) is also determined by the presence of e⁻···HO bonds just as found for $e^-(H_2O)_4$(**A**) and $e^-(H_2O)_8$(**A**) in solution. Whereas $e^-(H_2O)_{12}$(**B**) has 20 O···HO hydrogen bonds and four equivalent, weak e⁻···HO bonds and is formed from adding four water molecules (as a four-water ring) to the bottom of the $e^-(H_2O)_8$(**C**) structure, $e^-(H_2O)_{12}$(**A**) has 18 O···HO hydrogen bonds and two equivalent, strong e⁻···HO bonds and is formed from adding four water molecules (as a four-water ring) to the bottom of the $e^-(H_2O)_8$(**A**) structure. In view of the structural evolution from $e^-(H_2O)_4$(**A**) to $e^-(H_2O)_8$(**A**) and then to $e^-(H_2O)_{12}$(**A**), it appears that $e^-(H_2O)_8$(**A**) (and even $e^-(H_2O)_4$(**A**)) contains the basic structural feature that defines the fundamental chemical structure of the solvated electron in water.

The calculated most stable structures in solution can be compared with previous molecular dynamic simulations. Landman and co-workers[51,55,56,59−62,65] have performed extensive studies of the surface and internal states of the excess electron in water clusters. Their predicted vertical electron binding energies for the internal states are all considerably higher than those predicted for the corresponding surface states,[56] qualitatively consistent with the relative magnitudes of our calculated VDEs in Table 2. On the basis of our results, the most stable structures in solution all have the excess electron solvated internally or semiinternally and are always associated with the highest VDE values. Rossky et al.[27,28] reported the radial distribution functions of water oxygen atoms and water hydrogen atoms surrounding the hydrated electron. The coordination number of the hydrated electron obtained from integration of the radial correlation function depends on the choice of radial position used to determine the radius of the first solvation shell. When a radius of ~4 Å is used, the coordination number is about 6.[28] It is interesting to note that the first peak of the radial distribution function of water oxygen appears at 3.3 Å and that of the hydrogen appears at 2.3 Å.[27] When only the first peak is accounted for, the coordination number of the hydrated electron becomes 1.9 for the oxygen and 1.6 for the hydrogen;[27] both are close to the integer 2. This is qualitatively consistent with our optimized most stable structures $e^-(H_2O)_8$(**A**) and $e^-(H_2O)_{12}$(**A**) that each are associated with two strong e···HO bonds.

Electron Excitation Energies. The first three vertical electronic excitation energies calculated by using the CIS and TDDFT methods for the most stable $e^-(H_2O)_n$ structures, i.e., $e^-(H_2O)_4$(**A**), $e^-(H_2O)_8$(**A**), and $e^-(H_2O)_{12}$(**A**), are summarized in Table 5. The first excitation energies calculated at the

TABLE 5: The First Three Vertical Electron Excitation Energies (ΔE, eV) of the Solvated Electron in Water Calculated as Those of the Most Stable $e^-(H_2O)_n$ Structures in Water

	electron excitation energies		
calculation method[a]	$e^-(H_2O)_4$(**A**)	$e^-(H_2O)_8$(**A**)	$e^-(H_2O)_{12}$(**A**)
	Without Bulk Solvent Effects		
CIS/aug-cc-pVDZ+Ryd(O)	0.80, 0.81, 1.03		
CIS/cc-pVDZ+Ryd(O)	0.78, 0.79, 0.99	0.75, 0.97, 1.59	0.84, 1.09, 1.79
CIS/aug-cc-pVTZ+Ryd(O)	0.72, 0.73, 1.01		
CIS/cc-pVTZ+Ryd(O)	0.79, 0.80, 1.01		
TDDFT/cc-pVDZ+Ryd(O)	1.00, 1.02, 1.08	0.93, 1.16, 1.31	1.03, 1.29, 1.47
TDDFT/cc-pVTZ+Ryd(O)	1.01, 1.03, 1.07		
CAS(3,4)-MP2/cc-pVDZ+Ryd(O)	0.76	0.72	0.80
CAS(5,6)-MP2/cc-pVDZ+Ryd(O)	0.77		
CAS(3,4)-MP2/cc-pVTZ+Ryd(O)	0.80		
	With Bulk Solvent Effects		
CIS/aug-cc-pVDZ+Ryd(O)	0.96, 0.96, 1.16	1.07, 1.19, 1.99	1.06, 1.26, 2.10

[a] The CAS-MP2 calculations were performed only for the first excitation. The functional used in the TDDFT calculations is B3LYP.

CAS(3,4)-MP2 and CAS(5,6)-MP2 levels are also listed for comparison. These three excited states are all associated with electron excitations from the s-like SOMO to the p-like orbitals, consistent with previous description of the s→p excitations of the hydrated electron.[11,68] Our calculated results further show that the three p-like orbitals are not degenerate because the excess electron exists in a nonspherical, low-symmetry chemical environment. In order for the three p-like orbitals to be degenerate, the minimum symmetry requirement of the chemical environment of the solvated electron is the O_h or T_d point symmetry groups, whereas the $e^-(H_2O)_4$(**A**), $e^-(H_2O)_8$(**A**), and $e^-(H_2O)_{12}$(**A**) structures are all associated with the C_2 point group.

The three vertical electronic excitation energies calculated for the $e^-(H_2O)_4$(**A**) cluster in the gas phase are all larger than the corresponding VDE value, suggesting a dissociation process for the excess electron in the excited states of $e^-(H_2O)_4$(**A**) and that these VDE values refer to excitations to the continuum. However, these excited states are electron-bound in solution. The gas-phase values are only to be considered to be part of the excitation energies of the possible $e^-(H_2O)_4$(**A**) structure existing in solution (the last line in Table 5). The vertical electronic excitation energies calculated for $e^-(H_2O)_8$(**A**) and $e^-(H_2O)_{12}$(**A**) are all smaller than the corresponding VDE values. These excited states in $e^-(H_2O)_8$(**A**) and $e^-(H_2O)_{12}$(**A**) are electron-bound in both the gas phase and solution.

The data in Table 5 indicate that for whatever method used to calculate the excited states, as long as Rydberg functions are used, the diffuse functions in the standard correlation-consistent basis sets are not important and increasing the basis set from double-ζ to triple-ζ does not dramatically change the calculated results. The cc-pVDZ+Ryd(O) basis set appears to be adequate for calculating these excited states. The CAS-MP2 result is rather insensitive to the size of the active space used in the CAS calculation, suggesting that the CAS(3,4)-MP2 results are reliable and can be used as a benchmark to assess the CIS and TDDFT results. The CIS/cc-pVDZ+Ryd(O) results are all very close to the corresponding CAS(3,4)-MP2/cc-pVDZ+Ryd(O) results, whereas the TDDFT/cc-pVDZ+Ryd(O) results differ from the corresponding CAS(3,4)-MP2/cc-pVDZ+Ryd(O) results by ~0.2 eV.

It is likely that the shifts of the excitation energies from the gas phase to solution are overestimated because the fast relaxation of the excited state solvation was neglected in our calculations of the excited states. Nevertheless, the bulk solvent shifts are only a few tenths of an eV. The question that we are trying to answer is whether the first three electronic excitations of the most stable $e^-(H_2O)_n$ structures in aqueous solution are within the expected range of the photoabsorption observed for the hydrated electron in water. As shown in Table 5, neglecting the bulk solvent effects, the first three excitation energies calculated at all the levels for the largest cluster, $e^-(H_2O)_{12}$(**A**), are between 0.80 and 1.79 eV. Including the bulk solvent effects, these excitation energies are predicted to be between 0.9 and 2.1 eV. The estimated first three excitation energies are within the observed absorption range from 0.8 to 3.0 eV,[1,2] providing further evidence that the most stable structures of the hydrated electron that we have calculated are reasonable.

TABLE 6: The Absolute Hydration Free Energy of the Electron ($\Delta G_{Hyd}[e^-,n]$, in kcal/mol) Calculated as the Gibbs Free Energy Change from e^-(g, 1 mol/L) + $(H_2O)_n$(aq) to $e^-(H_2O)_n$ (aq) at $T = 298$ K

	Gibbs free energy change		
calculation method[a]	$n = 4$	$n = 8$	$n = 12$
bulk solvent shift	−32.3	−34.2	−29.5
MP2/6-31++G**	−28.3	−29.3	−29.4
MP2/aug-cc-pVDZ	−31.2	−32.0	−32.1
MP2/aug-cc-pVTZ	−31.8	−32.5	−32.5
MP2/aug-cc-pVQZ	−32.3	−32.9	
MP2/CBS	−32.5	−33.2	
CCSD/aug-cc-pVDZ	−32.7	−34.3	
CCSD/aug-cc-pVTZ	−33.2		
CCSD(T)/aug-cc-pVDZ	−32.7		
CCSD(T)/aug-cc-pVTZ	−33.3		
best estimate[b]	−34.0	**−35.5**	

[a] Computational method used for the gas-phase energy calculations. Bulk solvent shifts were calculated by using the SVPE approach at the MP2/6-31++G** level. All energy calculations were performed by using the geometries optimized at the B3LYP/6-31++G** level. [b] The best estimate is the MP2/CBS value plus the higher order electron correlation correction estimated as described in the text.

Free Energies of Solvation. The Gibbs free energy results calculated for $n = 4$, 8, and 12 using the most stable geometries optimized at the B3LYP/6-31++G** level are summarized in Table 6. The standard states of the electron used to obtain the values listed in Table 6 are consistent with those used by Jortner and Noyes,[34] i.e., both the gaseous and solvated electron are at one mole per liter with $T = 298$ K. If the standard state of the gaseous electron is 22.4 mol/L corresponding to the hypothetical ideal gas existing at $T = 298$ K and $P = 1$ atm, then a value of 1.89 kcal/mol should be added to all of the values listed in Table 6.

As shown in Table 6, the bulk solvent effects dominate the calculated hydration free energies; for $n = 4$ and 8, nearly all of the hydration free energy is due to the bulk solvent effect

contributions. This is qualitatively consistent with the results obtained from the path-integral molecular dynamics simulations on the excess electron in water clusters by Barnett et al.[56] Their results indicate that the convergence of the calculated properties to the bulk limit is rather slow, which is a manifestation of the role of long-range interactions in electron solvation in polar solvents.[56]

The convergence of our calculated hydration free energy with respect to n can be examined by comparing the results calculated at the same level of theory for different n values. As shown in Table 6, there is a small change, ~1 kcal/mol, in the calculated hydration free energy from $n = 4$ to $n = 8$. The change in energy from $n = 8$ to $n = 12$ is negligible, within 0.1 kcal/mol, based on the energy calculations at the MP/6-31++G**, MP2/aug-cc-pVDZ, and MP2/aug-cc-pVTZ levels. The convergence with respect to n does not depend strongly on the level of theory used for the gas-phase calculations.

Because the hydration free energy calculations are well converged at $n = 8$ for the solvated electron, we just need to perform as high-level energy calculations as possible on the aqueous clusters up to $n = 8$. The CCSD(T) method can predict total molecular dissociation energies involving covalent bonds to better than 1 kcal/mol[131,190,191] when sufficiently large basis sets are used and the valence electron correlation energy is extrapolated to the complete basis set (CBS) limit and if other effects such as core−valence correlation, relativity, and zero-point energies are properly accounted for. The MP2 method has been shown to give very good energies for hydrogen-bonded systems.[188,189,192] We extrapolate the MP2 energies to the CBS limit by using the augmented correlation-consistent basis sets, aug-cc-pVDZ, aug-cc-pVTZ, and aug-cc-pVQZ with eq 7. The extrapolated MP2/CBS results lead to $\Delta G_{hyd}[e^-,4] = -32.5$ kcal/mol and $\Delta G_{hyd}[e^-,8] = -33.2$ kcal/mol. We were unable to complete CCSD(T) energy calculations on $e^-(H_2O)_8$(**A**) using the augmented correlation-consistent basis sets due to hardware and software limitations, but we were able to carry out a CCSD energy calculation on $e^-(H_2O)_8$(**A**) with the aug-cc-pVDZ basis set and CCSD(T) calculations on $e^-(H_2O)_4$(**A**) with the aug-cc-pVDZ and aug-cc-pVTZ basis sets. The calculated results for $n = 4$ show that the hydration free energies calculated at the CCSD(T) level are nearly identical to 0.1 kcal/mol to the corresponding values calculated at the CCSD level for both the aug-cc-pVDZ and aug-cc-pVTZ basis set. For $n = 4$, we estimate that $\Delta G_{hyd}(e^-)$ is −34.0 kcal/mol, obtained by adding the difference between CCSD(T) and MP2 energies of 1.5 kcal/mol with the aug-cc-pVTZ basis set to the MP2/CBS value. We note that the correction factor is the same independent of whether it is corrected by using CCSD or CCSD(T) method or the aug-cc-pVDZ or aug-cc-pVTZ basis set. For $n = 8$, we estimate that $\Delta G_{hyd}(e^-)$ is −35.5 kcal/mol obtained as the sum of the MP2/CBS value and the change, −2.3 kcal/mol, from the MP2/aug-cc-pVDZ value to the CCSD/aug-cc-pVDZ value. Thus, our best estimate of the absolute hydration free energy of the electron $\Delta G_{hyd}^{298}(e^-)$ is −35.5 kcal/mol for the above-defined standard state. This predicted $\Delta G_{hyd}^{298}(e^-)$ value is 3.9 kcal/mol higher than the corresponding value of −39.4 kcal/mol estimated by Jortner and Noyes,[34] based on the extrapolated results of monatomic cations.[35] Our calculated value is 0.9 kcal/mol lower than and in excellent agreement with the most recent value of-34.6 kcal/mol derived by Bartels.[38]

How can we test our prediction for $\Delta G_{hyd}^{298}(e^-)$? The predicted $\Delta G_{hyd}^{298}(e^-)$ value of −35.5 kcal/mol combined with our previously predicted $\Delta G_{hyd}^{298}(H^+)$ value of −262.4 kcal/mol[121] and $\Delta G_{hyd}^{298}(HO^-)$ value of −104.5 kcal/mol[122] by using the same computational protocol gives $\Delta G_{hyd}^{298}(e^-) + \Delta G_{hyd}^{298}(H^+) = -297.9$ kcal/mol and $\Delta G_{hyd}^{298}(e^-) - \Delta G_{hyd}^{298}(HO^-) = 69.0$ kcal/mol. The predicted $\Delta G_{hyd}^{298}(e^-) + \Delta G_{hyd}^{298}(H^+)$ and $\Delta G_{hyd}^{298}(e^-) - \Delta G_{hyd}^{298}(HO^-)$ values can be tested by appropriate combinations of available experimental thermodynamic data. We can derive the $\Delta G_{hyd}^{298}(e^-) + \Delta G_{hyd}^{298}(H^+)$ and $\Delta G_{hyd}^{298}(e^-) - \Delta G_{hyd}^{298}(HO^-)$ values from well-established experimental thermodynamic data. Thus, we need to know the free energies of following reactions/changes:

$$H_2O(l, \text{i.e., } 55.5 \text{ M}) + e^-(aq, 1 \text{ M}) \rightarrow H(aq, 1 \text{ M}) + HO^-(aq, 1 \text{ M}) \quad (8)$$

$$H_2O(l, \text{i.e., } 55.5 \text{ M}) \rightarrow H^+(aq, 1 \text{ M}) + HO^-(aq, 1 \text{ M}) \quad (9)$$

$$e^-(g, 1/22.4 \text{ mol/L}) \rightarrow e^-(g, 1 \text{ mole/L}) \quad (10)$$

$$H^+(g, 1/22.4 \text{ mol/L}) + e^-(g, 1/22.4 \text{ mol/L}) \rightarrow H(g, 1/22.4 \text{ mol/L}) \quad (11)$$

$$H(g, 1/22.4 \text{ mol/L}) \rightarrow H(aq, 1 \text{ M}) \quad (12)$$

$$H_2O(L, \text{i.e., } 55.5 \text{ M}) \rightarrow H_2O(g, 1/22.4 \text{ mol/L}) \quad (13)$$

$$H_2O(g, 1/22.4 \text{ mol/L}) \rightarrow H^+(g, 1/22.4 \text{ mol/L}) + HO^-(g, 1/22.4 \text{ mol/L}) \quad (14)$$

The value of $\Delta G^{298}(8) = 5.87$ kcal/mol is based on well-established experimental data.[34] From the established experimental thermodynamic equilibration of water autoionization, $\Delta G^{298}(9) = 19.09$ kcal/mol. $\Delta G^{298}(10) = 1.89$ kcal/mol is easily determined from the contribution of the standard entropy change to the Gibbs free energy. $\Delta G^{298}(11) = -313.58$ kcal/mol (13.59844 eV)[130] is the ionization potential for the H atom. $\Delta G^{298}(12) = 4.5$ kcal/mol was estimated by Jortner and Noyes[34] on the basis of the experimental ΔG^{298}[He (g, 1/22.4 mol/L) → He (aq, 1 M)] value of 4.67 kcal/mol and the experimental ΔG^{298}[H_2 (g, 1/22.4 mol/L) → H_2 (aq, 1 M)] value of 4.24 kcal/mol. The NBS (now NIST) tables[193] provide $\Delta G^{298}(13) = 2.05$ kcal/mol. The experimental $\Delta G^{298}(14)$ value is 384.1 ± 0.2 kcal/mol, based on the NIST Standard Reference Database.[130] Very recently, this $\Delta G^{298}(14)$ value has been revised to 383.61 ± 0.07 kcal/mol, due to a combination of new sophisticated experimental and computational results for the heat of formation of the OH radical which revised this value by almost 0.5 kcal/mol.[131,132]

Using the above thermodynamic data, we obtain

$$\Delta G_{hyd}^{298}(e^-) + \Delta G_{hyd}^{298}(H^+) = \Delta G^{298}(9) + \Delta G^{298}(11) + \Delta G^{298}(12) - \Delta G^{298}(8) - \Delta G^{298}(10) = -297.8 \text{ kcal/mol}$$

in excellent agreement with our predicted $\Delta G_{hyd}^{298}(e^-) + \Delta G_{hyd}^{298}(H^+)$ value of −297.9 kcal/mol. The above thermodynamic data also lead to

$$\Delta G_{hyd}^{298}(e^-) - \Delta G_{hyd}^{298}(HO^-) = \Delta G^{298}(11) + \Delta G^{298}(12) + \Delta G^{298}(13) + \Delta G^{298}(14) - \Delta G^{298}(8) - \Delta G^{298}(10) =$$
$$68.8 \pm 0.1 \text{ kcal/mol (based on the latest } \Delta G^{298}(14) \text{ value)}$$
$$\text{or } 69.3 \pm 0.2 \text{ kcal/mol (based on the NIST-listed } \Delta G^{298}(14) \text{ value)},$$

in excellent agreement with our predicted $\Delta G_{hyd}^{298}(e^-) - \Delta G_{hyd}^{298}(HO^-)$ value of 69.0 kcal/mol. Such excellent agreement

strongly suggests that our calculated value for $\Delta G_{hyd}^{298}(e^-)$ is reliable. This, in turn, suggests that our most stable $e^-(H_2O)_n$ structures, exemplified by $e^-(H_2O)_4$(**A**), $e^-(H_2O)_8$(**A**), and $e^-(H_2O)_{12}$(**A**), each with two strong e···HO bonds, indeed represents the fundamental structural and bonding characteristics of the solvated electron in water.

Conclusion

A series of electronic structure calculations have been performed to determine possible stable structures for the hydrated electron and to determine its absolute hydration free energy, $\Delta G_{hyd}^{298}(e^-)$. The calculated results indicate that both the thermal motion and bulk solvent effects can qualitatively change the relative thermodynamic stability of different possible structures of the hydrated electron, and that the most stable structure in solution is not necessarily the most stable structure in the gas phase. The most stable structure in solution based on our hybrid supermolecule-continuum approach reveals a unique feature of the chemical nature of the solvated electron in water, i.e., the electron forms two strong electron-hydrogen bonds of the e⁻···HO type with the hydrogen-bonded water cluster and two of the hydrogen bonds in the neutral water cluster are broken to accommodate these new bonds.

On the basis of the most stable structures, the calculated electronic excitation energies are within the observed absorption range of the hydrated electron in water. The absolute hydration free energy of the solvated electron in water has been calculated to be −35.5 kcal/mol by using a reliable computational protocol of first-principles solvation-included electronic structure calculations, the same approach recently used to calculate the absolute hydration free energy of the proton and hydroxide ion. This value is in excellent agreement with the derived experimental value of −34.6 kcal/mol.[38] The predicted $\Delta G_{hyd}^{298}(e^-)$ value of −35.5 kcal/mol combined with our previously predicted $\Delta G_{hyd}^{298}(H^+)$ value of −262.4 kcal/mol[28] and $\Delta G_{hyd}^{298}(HO^-)$ value of −104.5 kcal/mol by using the same computational protocol gives $\Delta G_{hyd}^{298}(e^-) + \Delta G_{hyd}^{298}(H^+) = -297.9$ kcal/mol and $\Delta G_{hyd}^{298}(e^-) - \Delta G_{hyd}^{298}(HO^-) = 69.0$ kcal/mol in excellent agreement with the corresponding values derived from available experimental data. These structural and energetic results, together with the use of the e⁻···HO bond concept, provide a fundamental basis for future investigations of the thermodynamic properties and detailed reaction mechanisms of the hydrated electron.

Acknowledgment. This research was performed in the William R. Wiley Environmental Molecular Sciences Laboratory (EMSL) and part of the work was done using the Molecular Sciences Computing Facility (MSCF) in the EMSL at PNNL. The EMSL, including the MSCF, is a national user facility funded by the Office of Biological and Environmental Research of the U.S. Department of Energy. This work was supported by the U.S. Department of Energy, Office of Basic Energy Sciences, Geosciences Research Program, and the Office of Biological and Environmental Research. PNNL is a multiprogram national laboratory operated by Battelle Memorial Institute for the U.S. Department of Energy.

Supporting Information Available: The optimized geometries of the anionic cluster structures and the corresponding energies, zero-point vibration energies, dipole moments, and quadrupole moments are provided. This material is available free of charge via the Internet at http://pubs.acs.org.

References and Notes

(1) Hart, E. J.; Anbar, M. *The Hydrated Electron*; Wiley: New York, 1970.
(2) Hart, E. J.; Boag, J. W. *J. Am. Chem. Soc.* **1962**, *84*, 4090.
(3) Schmidt, K. H.; Han, P.; Bartels, D. M. *J. Phys. Chem.* **1992**, *96*, 199.
(4) Renou, F.; Mostafavi, M. *Chem. Phys. Lett.* **2001**, *335*, 363.
(5) Experimental reactivity data for a total of 1891 reactions of the hydrated electron have been collected in the web site (http://www.rcdc.nd.edu/compilations/Eaq/Eaq.htm) together with the original literature source. See references therein.
(6) Long, F. H.; Lu, H.; Eisenthal, K. B. *Phys. Rev. Lett.* **1990**, *64*, 1469.
(7) Gauduel, Y.; Pommeret, S.; Antonetti, A. *J. Phys. Chem.* **1993**, *97*, 134.
(8) Assel, M.; Laenen, R.; Laubereau, A. *Chem. Phys. Lett.* **2000**, *317*, 13.
(9) Sander, M. U.; Luther, K.; Troe, J. *Ber. Bunsen-Ges. Phys. Chem.* **1993**, *97*, 953.
(10) Thomsen, C. L.; Madsen, D.; Keiding, S. R.; Thøgersen, J.; Christiansen, O. *J. Chem. Phys.* **1999**, *110*, 3453.
(11) Baltuska, A.; Emde, M. F.; Pshenichnikov, M. S.; Wiersma, D. A. *J. Phys. Chem. A* **1999**, *103*, 10065.
(12) Laenen, R.; Roth, T.; Laubereau, A. *Phys. Rev. Lett.* **2000**, *85*, 50.
(13) Lehr, L.; Zanni, M. T.; Frischkorn, C.; Weinkauf, R.; Neumark, D. M. *Science*, **1999**, *284*, 635.
(14) Kläning, U. K.; Byberg, J. R.; Sehested, K. *J. Phys. Chem. A* **1999**, *103*, 5055.
(15) Saleh, N.; Flippo, K.; Nemoto, K.; Umstadter, D. *Rev. Sci. Instrum.* **2000**, *71*, 2000.
(16) Mizuno, M.; Tahara, T. *J. Phys. Chem. A* **2001**, *105*, 8823.
(17) Kee, T. W.; Son, D. H.; Kambhampati, P.; Barbara, P. F. *J. Phys. Chem. A* **2001**, *105*, 8434.
(18) Tauber, M.; Mathies, R. *J. Phys. Chem. A* **2001**, *105*, 10952.
(19) Kambhampati, P.; Son, D. H.; Kee, T. W.; Barbara, P. F. *J. Phys. Chem. A* **2001**, *106*, 2374.
(20) Tauber, M. J.; Mathies, R. A. *Chem. Phys. Lett.* **2002**, *354*, 518.
(21) Miller, A. D.; Bezel, I.; Gaffney, K. J.; Garrett-Roe, S.; Liu, S. H.; Szymanski, P.; Harris, C. B. *Science* **2002**, *297*, 1163.
(22) Feng, D.-F.; Kevan, L. *Chem. Rev.* **1980**, *80*, 1 and references therein.
(23) Kevan, L. *Acc. Chem. Res.* **1981**, *14*, 138 and references therein.
(24) Fueki, K.; Feng, D.-F.; Kevan, L. *J. Am. Chem. Soc.* **1973**, *95*, 1398.
(25) Gaathon, A.; Jortner, J. In *Electrons in Fluids*; Jortner, J., Kestner, N. R., Eds.; Springer: Berlin, 1973; p 429.
(26) Copeland, D. A.; Kestner, N. R.; Jortner, J. *J. Chem. Phys.* **1970**, *53*, 1189.
(27) Schnitker, J.; Rossky, P. J. *J. Chem. Phys.* **1987**, *86*, 3471.
(28) Rossky, P. J.; Schnitker, J. *J. Phys. Chem.* **1988**, *92*, 4277.
(29) Hameka, H. F.; Robinson, G. W.; Marsden, C. J. *J. Phys. Chem.* **1987**, *91*, 3150.
(30) Symons, M. C. R. *J. Phys. Chem.* **1988**, *92*, 7260.
(31) Muguet, F.; Bassez, M.-P.; Robinson, G. W. J. *J. Phys. Chem.* **1988**, *92*, 7262.
(32) Tuttle, T. R., Jr.; Golden, S. *J. Phys. Chem.* **1991**, *95*, 5725.
(33) Sobolewski, A.; Domcke, W. *Phys. Chem. Chem. Phys.* **2002**, *4*, 4.
(34) Jortner, J.; Noyes, R. M.; *J. Phys. Chem.* **1966**, *70*, 770.
(35) Noyes, R. M. *J. Am. Chem. Soc.* **1964**, *86*, 971.
(36) Shiraishi, H.; Sunaryo, G. R.; Ishigure, K. *J. Phys. Chem.* **1994**, *98*, 5164.
(37) Coe, J. V. *Int. Rev. Phys. Chem.* **2001**, *20*, 33.
(38) Bartels, D. M. Unpublished result (private communication).
(39) Conway, B. E. *Ionic Hydration in Chemistry and Biophysics*; Elsevier: New York, 1981.
(40) Marcus, Y. *Ion Solvation*; Wiley: New York, 1985.
(41) Klots, C. E. *J. Phys. Chem.* **1981**, *85*, 3585.
(42) Tissandier, M. D.; Cowen, K. A.; Feng, W. Y.; Gundlach, E.; Cohen, M. H.; Earhart, A. D.; Coe, J. V. *J. Phys. Chem. A* **1998**, *102*, 7787.
(43) Tawa, G. J.; Topol, I. A.; Burt, S. K.; Caldwell, R. A.; Rashin, A. A. *J. Chem. Phys.* **1998**, *109*, 4852.
(44) Mejias, J. A.; Lago, S. *J. Chem. Phys.* **2000**, *113*, 7306.
(45) Friedman, H. L.; Krishnan, V. V. *Water: A Comprehensive Treatise*; Plenum: New York, 1973.
(46) Zhu, T.; Li, J.; Hawkins, G. D.; Cramer, C. J.; Truhlar, D. G. *J. Chem. Phys.* **1998**, *109*, 9117.
(47) Hall, R. W.; Wolynes, P. G. *Phys. Rev. B* **1986**, *33*, 7879.
(48) Schnitker, J. S.; Rossky, P. J.; Kenney-Wallace, G. *J. Chem. Phys.* **1986**, *85*, 2986.
(49) Schnitker, J.; Rossky, P. J. *J. Chem. Phys.* **1987**, *86*, 3462.
(50) Schnitker, J. S.; Motakabbir, A. K.; Rossky, P. J.; Friesner, R. A. *Phys. Rev. Lett.* **1988**, *60*, 456.
(51) Barnett; R. N.; Landman, U.; Cleveland, C. L.; Jortner, J. *Phys. Rev. Lett.* **1987**, *59*, 811.

(52) Sprik, M.; Klein, M. L. *J. Chem. Phys.* **1988**, *89*, 1592.
(53) Barnett; R. N.; Landman, U.; Nitzan, A. *J. Chem. Phys.* **1988**, *89*, 2242.
(54) Barnett; R. N.; Landman, U.; Nitzan, A. *Phys. Rev. A* **1988**, *38*, 2178.
(55) Barnett; R. N.; Landman, U.; Cleveland, C. L.; Jortner, J. *J. Chem. Phys.* **1988**, *88*, 4421.
(56) Barnett; R. N.; Landman, U.; Cleveland, C. L.; Jortner, J. *J. Chem. Phys.* **1988**, *88*, 4429.
(57) Motakabbir, K. A.; Rossky, P. J. *Chem. Phys*. **1989**, *129*, 253.
(58) Schnitker, J.; Rossky, P. J. *J. Phys. Chem*. **1989**, *93*, 6965.
(59) Barnett; R. N.; Landman, U.; Nitzan, A. *Phys. Rev. Lett.* **1989**, *62*, 106.
(60) Barnett; R. N.; Landman, U.; Makov, G. *J. Chem. Phys.* **1990**, *93*, 6226.
(61) Barnett; R. N.; Landman, U.; Nitzan, A. *J. Chem. Phys.* **1990**, *93*, 8187.
(62) Neria, E.; Nitzan, A.; Barnett; R. N.; Landman, U. *Phys. Rev. Lett.* **1991**, *67*, 1011.
(63) Webster, F.; Schnitker, J.; Friedrichs, M.; Friesner, R. A.; Rossky, P. J. *Phys. Rev. Lett*. **1991**, *66*, 3172.
(64) Del Buono, G. S.; Rossky, P. J.; Murphrey, T. H. *J. Phys. Chem*. **1992**, *96*, 7761.
(65) Kaukonen, H.-P.; Barnett; R. N.; Landman, U. *J. Chem. Phys.* **1992**, *97*, 1365.
(66) Keszei, E.; Nagy, S.; Murphrey, T. H.; Rossky, P. J. *J. Chem. Phys*. **1993**, *99*, 2004.
(67) Schwartz, B. J.; Rossky, P. J. *Phys. Rev. Lett*. **1994**, *72*, 3282.
(68) Schwartz, B. J.; Rossky, P. J. *J. Chem. Phys.* **1994**, *101*, 6902.
(69) Schwartz, B. J.; Rossky, P. J. *J. Chem. Phys.* **1994**, *101*, 6917.
(70) Schwartz, B. J.; Rossky, P. J. *J. Phys. Chem*. **1994**, *98*, 4489.
(71) Rosenthal, S. J.; Schwartz, B. J.; Rossky, P. J. *Chem. Phys. Lett*. **1994**, *229*, 443.
(72) Keszei, E.; Murphrey, T. H.; Rossky, P. J. *J. Phys. Chem*. **1995**, *99*, 22.
(73) Staib, A.; Borgis, D. *J. Chem. Phys.* **1995**, *103*, 2642.
(74) Schwartz, B. J.; Rossky, P. J. *J. Phys. Chem*. **1995**, *99*, 2953.
(75) Pimblott, S. M.; LaVerne, J. A.; Bartels, D. M.; Jonah, C. D. *J. Phys. Chem.* **1996**, *100*, 9412.
(76) Crowell, R. A.; Bartels, D. M. *J. Phys. Chem.* **1996**, *100*, 17713.
(77) Crowell, R. A.; Bartels, D. M. *J. Phys. Chem.* **1996**, *100*, 17940.
(78) Schwartz, B. J.; Rossky, P. J. *J. Chem. Phys.* **1996**, *105*, 6997.
(79) Prezhdo, O. V.; Rossky, P. J. *J. Phys. Chem*. **1996**, *100*, 17094.
(80) Turi, L.; Mosyak, A.; Rossky, P. J. *J. Chem. Phys*. **1997**, *107*, 1970.
(81) Mosyak, A. A.; Prezhdo, O. V.; Rossky, P. J. *J. Chem. Phys.* **1998**, *109*, 6390.
(82) Bartels, D. M. *J. Chem. Phys.* **2001**, *115*, 4404.
(83) Yang, C.-Y.; Wong, K. F.; Skaf, M. S.; Rossky, P. J. *J. Chem. Phys*. **2001**, *114*, 3598.
(84) Wong, K. F.; Rossky, P. J. *J. Phys. Chem. A* **2001,** *105*, 2546.
(85) Wong, K. F.; Rossky, P. J. *J. Chem. Phys*. **2002**, *116*, 8418.
(86) Wong, K. F.; Rossky, P. J. *J. Chem. Phys*. **2002**, *116*, 8429.
(87) Takahashi, K.; Bartels, D. M.; Cline, J. A. *Chem. Phys. Lett*. **2002**, *357*, 358.
(88) Chipman, D. M. *J. Phys. Chem*. **1979**, *83*, 1657.
(89) Barnett, R. N.; Landman, U.; Dhar, S.; Kestner, N. R.; Jortner, J.; Nitzan, A. *J. Chem. Phys.* **1989**, *91*, 7797.
(90) Kim, K. S.; Park, I.; Lee, S.; Cho, K.; Lee, J. Y.; Kim, J.; Joannopoulos, J. D. *Phys. Rev. Lett.* **1996**, *76*, 956.
(91) Lee, S.; Lee, S. J.; Lee, J. Y.; Kim, J.; Kim, K. S.; Park, I.; Cho, K.; Joannopoulos, J. D. *Chem. Phys. Lett.* **1996**, *254*, 128.
(92) Kim, K. S.; Lee, S. J.; Kim, J.; Lee, J. Y. *J. Am. Chem. Soc.* **1997**, *119*, 9329.
(93) Lee, S.; Kim, J.; Lee. S. J.; Kim, K. S. *Phys. Rev. Lett.* **1997**, *79*, 2038.
(94) Kim, J.; Park, J. M.; Oh, K. S.; Lee, J. Y.; Lee, S.; Kim, K. S. *J. Chem. Phys.* **1997**, *106*, 10207.
(95) Smith, D. M. A.; Smets, J.; Elkadi, Y.; Adamowicz, L. *J. Chem. Phys.* **1997**, *107*, 5788.
(96) Smith, D. M. A.; Smets, J.; Elkadi, Y.; Adamowicz, L. *J. Chem. Phys.* **1998**, *109*, 1238.
(97) Bouteiller, Y.; Desfrancois, C.; Schermann, J. P.; Latajka, Z.; Silvi, B. *J. Chem. Phys.* **1998**, *108*, 7967.
(98) Tsurusawa, T.; Iwata, S. *Chem. Phys. Lett.* **1998**, *287*, 553.
(99) Kim, J. K.; Suh, S. B.; Kim, K. S. *J. Chem. Phys.* **1999**, *111*, 10077.
(100) Tsurusawa, T.; Iwata, S. *Chem. Phys. Lett.* **2000**, *315*, 433.
(101) Lee, H. M.; Kim, K. S. *J. Chem. Phys.* **2002**, *117*, 706.
(102) Gutowski, M.; Skurski, P. *Recent Res. Dev. Phys. Chem.* **1999**, *3*, 245.
(103) Alfonso, D. R.; Jordan, K. D. *J. Chem. Phys.* **2002**, *116*, 3612.
(104) Haberland, H.; Ludewigt, C.; Schindler, H.-G.; Worsnop, D. R. *J. Phys. Chem.* **1984**, *88*, 3903.
(105) Haberland, H.; Ludewigt, C.; Schindler, H.-G.; Worsnop, D. R. *J. Chem. Phys.* **1984**, *81*, 3742.
(106) Desfrancois, C.; Khelifa, N.; Lisfi, A.; Schermann, J. P.; Eaton, J. G.; Bowen, K. H. *J. Chem. Phys.* **1985**, *95*, 1991.
(107) Posey, L. A.; Deluca, M. J.; Campagnola, P. J.; Johnson, M. A. *J. Phys. Chem.* **1989**, *93*, 1178.
(108) Arnold, S. T.; Morris, R. A.; Viggiano, A. A.; Johnson, M. A. *J. Phys. Chem.* **1996**, *100*, 2900.
(109) Castleman, A. W.; Bowen, K. H. *J. Phys. Chem.* **1996**, *100*, 12911.
(110) Coe, J. V.; Lee, G. H.; Eaton, J. G.; Arnold, S. T.; Sarkas, H. W.; Bowen, K. H. Ludewigt, C.; Haberland, H.; Worsnop, D. R. *J. Chem. Phys.* **1990**, *92*, 3980.
(111) Lee, G. H.; Arnold, S. T.; Eaton, J. G.; Sarkas, H. W.; Bowen, K. H. Ludewigt, C.; Haberland, H. *Z. Phys. D* **1991**, *20*, 9.
(112) Bailey, C. G.; Kim, J.; Johnson, M. A. *J. Phys. Chem.* **1996**, *100*, 16782.
(113) Desfrancois, C.; Baillon, B.; Schermann, J. P.; Arnold, S. T.; Hendricks, J. H.; Bowen, K. H. *Phys. Rev. Lett.* **1994**, *72*, 48.
(114) Bailey, C. G.; Johnson, M. A. *Chem. Phys. Lett.* **1997**, *265*, 185.
(115) Bailey, C. G.; Johnson, M. A. *J. Chem. Phys.* **1997**, *106*, 811.
(116) Ayotte, P.; Bailey, C. G.; Kim, J.; Johnson, M. A. *J. Chem. Phys.* **1998**, *108*, 444.
(117) Kim, J.; Becker, I.; Cheshnovsky, O.; Johnson, M. A. *Chem. Phys. Lett.* **1998**, *297*, 90.
(118) Ayotte, P.; Weddle, G. H.; Bailey, C. G.; Johnson, M. A.; Vila, F.; Jordan, K. D. *J. Chem. Phys.* **1999**, *110*, 6268.
(119) Kelly, J. A.; Weddle, G. H.; Robertson, W. H.; Johnson, M. A. *J. Chem. Phys.* **2002**, *116*, 1201.
(120) Zhan, C.-G.; Landry, D. W.; Ornstein, R. L. *J. Am. Chem. Soc*. **2000**, *122*, 2621.
(121) Zhan, C.-G.; Dixon, D. A. *J. Phys. Chem. A* **2001**, *105*, 11534.
(122) Zhan, C.-G.; Dixon, D. A. *J. Phys. Chem. A* **2002**, *106*, 9737.
(123) Zhan, C.-G.; Bentley, J.; Chipman, D. M. *J. Chem. Phys.* **1998**, *108*, 177.
(124) Zhan, C.-G.; Chipman, D. M. *J. Chem. Phys.* **1998**, *109*, 10543.
(125) Zhan, C.-G.; Chipman, D. M. *J. Chem. Phys.* **1999**, *110*, 1611.
(126) Zhan, C.-G.; Landry, D. W.; Ornstein, R. L. *J. Phys. Chem. A* **2000**, *104*, 7672.
(127) Zhan, C.-G.; Norberto de Souza, O.; Rittenhouse, R.; Ornstein, R. L. *J. Am. Chem. Soc.* **1999**, *121*, 7279.
(128) Zhan, C.-G.; Zheng, F. *J. Am. Chem. Soc*. **2001**, *123*, 2835.
(129) Zhan, C.-G.; Niu, S.; Ornstein, R. L. *J. Chem. Soc., Perkin Trans. 2* **2001**, *1*, 23.
(130) Mallard, W. G.; Linstrom, P. J., Eds. NIST Chemistry WebBook, NIST Standard Reference Database Number 69 February 2000; National Institute of Standards and Technology: Gaithersburg, MD, 2000 (http://webbook.nist.gov).
(131) Ruscic, B.; Feller, D.; Dixon, D. A.; Peterson, K. A.; Harding, L. B.; Asher, R. L.; Wagner, A. F. *J. Phys. Chem. A* **2001**, *105*, 1.
(132) Ruscic, B.; Wagner, A. F.; Harding, L. B.; Asher, R. L.; Feller, D.; Dixon, D. A.; Peterson, K. A.; Song, Y.; Qian, X.; Ng, C.-Y.; Liu, J.; Chen, W.; Schwenke, D. W. *J. Phys. Chem. A.* **2002**, *106*, 2727.
(133) Becke, A. D. *J. Chem. Phys.* **1993**, *98*, 5648.
(134) Lee, C.; Yang, W.; Parr, R. G. *Phys. Rev. B* **1988**, *37*, 785.
(135) Stephens, P. J.; Devlin, F. J.; Chabalowski, C. F.; Frisch, M. J. *J. Phys. Chem.* **1994**, *98*, 11623.
(136) Hehre, W. J.; Radom, L.; Schleyer, P. v. R.; Pople, J. A. *Ab Initio Molecular Orbital Theory*; John Wiley & Sons: New York, 1986.
(137) Hamad, S.; Lago, S.; Mejias, J. A. *J. Phys. Chem. A* **2002**, *106*, 9104.
(138) Dunning, T. H. Jr. *J. Chem. Phys.* **1989**, *90*, 1007.
(139) Kendall, R. A.; Dunning, T. H., Jr.; Harrison, R. J. *J. Chem. Phys*. **1992**, *96*, 6796.
(140) Peterson, K. A.; Wood, D. E.; Dunning, T. H., Jr. *J. Chem. Phys*. **1994**, *100*, 7410.
(141) Woon, D. E.; Dunning, T. H., Jr. *J. Chem. Phys.* **1995**, *103*, 4572.
(142) Purvis, G. D., III; Bartlett, R. J. *J. Chem. Phys*. **1982**, *76*, 1910.
(143) Raghavachari, K.; Trucks, G. W.; Pople, J. A.; Head-Gordon, M. *Chem. Phys. Lett*. **1989**, *157*, 479.
(144) Watts, J. D.; Gauss, J.; Bartlett, R. J. *J. Chem. Phys*. **1993**, *98*, 8718.
(145) Tomasi, J.; Persico, M. *Chem. Rev.* **1994**, *94*, 2027.
(146) Zhan, C.-G.; Landry, D. W. *J. Phys. Chem. A* **2001**, *105*, 1296.
(147) Zheng, F.; Zhan, C.-G.; Ornstein, R. L. *J. Chem. Soc. Perkin Trans. 2* **2001**, 2355.
(148) Zheng, F.; Zhan, C.-G.; Ornstein, R. L. *J. Phys. Chem. B* **2002**, *106*, 717.
(149) Zhan, C.-G.; Dixon, D. A.; Sabri, M. I.; Kim, M.-S.; Spencer, P. S. *J. Am. Chem. Soc.* **2002**, *124*, 2744.
(150) Dixon, D. A.; Feller, D.; Zhan, C.-G.; Francisco, S. F. *J. Phys. Chem. A* **2002**, *106*, 3191.
(151) Schmidt, M. W.; Baldridge, K. K.; Boatz, J. A.; Elbert, S. T.; Gordon, M. S.; Jensen, J. H.; Koseki, S.; Matsunaga, N.; Nguyen, K. A.;

Su, S. J.; Windus, T. L.; Dupuis, M.; Montgomery, J. A. *J. Comput. Chem.* **1993**, *14*, 1347.
(152) Cramer, C. J.; Truhlar, D. G. In *Solvent Effects and Chemical Reactions*; Tapia, O., Bertran, J., Eds.; Kluwer: Dordrecht, 1996; p 1.
(153) Chipman, D. M. *J. Chem. Phys.* **2000**, *112*, 5558.
(154) Barone, V.; Cossi, M.; Tomasi, J. *J. Chem. Phys.* **1997**, *107*, 3210.
(155) Tomasi, J.; Mennucci, B.; Cances, E. *J. Mol. Struct. (THEOCHEM)* **1999**, *464*, 211.
(156) Cancès, E.; Mennucci, B. *J. Chem. Phys.* **2001**, *114*, 4744.
(157) Cossi, M.; Rega, N.; Scalmani, G.; Barone, V. *J. Chem. Phys.* **2001**, *114*, 5691.
(158) Chipman, D. M. *J. Chem. Phys.* **2002**, *116*, 10129.
(159) Tawa, G. J.; Topol, I. A.; Burt, S. K.; Caldwell, R. A.; Rashin, A. A. *J. Chem. Phys.* **1998**, *109*, 4852.
(160) Topol, I. A.; Tawa, G. J.; Burt, S. K.; Rashin, A. A. *J. Chem. Phys.* **1999**, *111*, 10998.
(161) Cances, M. T.; Mennucci, B.; Tomasi, J. *J. Chem. Phys*. **1997**, *107*, 3032.
(162) Cossi, M.; Barone, V.; Mennucci, B.; Tomasi, J. *Chem. Phys. Lett.* **1998**, *286*, 253.
(163) Mennucci, B.; Cammi, R.; Tomasi, J. *J. Chem. Phys.* **1998**, *109*, 2798.
(164) Frisch, M. J.; Trucks, G. W.; Schlegel, H. B.; Scuseria, G. E.; Robb, M. A.; Cheeseman, J. R.; Zakrzewski, V. G.; Montgomery, J. A.; Stratmann, R. E.; Burant, J. C.; Dapprich, S.; Millam, J. M.; Daniels, A. D.; Kudin, K. N.; Strain, M. C.; Farkas, O.; Tomasi, J.; Barone, V.; Cossi, M.; Cammi, R.; Mennucci, B.; Pomelli, C.; Adamo, C.; Clifford, S.; Ochterski, J.; Petersson, G. A.; Ayala, P. Y.; Cui, Q.; Morokuma, K.; Malick, D. K.; Rabuck, A. D.; Raghavachari, K.; Foresman, J. B.; Cioslowski, J.; Ortiz, J. V.; Stefanov, B. B.; Liu, G.; Liashenko, A.; Piskorz, P.; Komaromi, I.; Gomperts, R.; Martin, R. L.; Fox, D. J.; Keith, T.; Al-Laham, M. A.; Peng, C. Y.; Nanayakkara, A.; Gonzalez, C.; Challacombe, M.; Gill, P. M. W.; Johnson, B.; Chen, W.; Wong, M. W.; Andres, J. L.; Gonzalez, A. C.; Head-Gordon, M.; Replogle, E. S.; Pople, J. A. *Gaussian 98*, revision A.6; Gaussian, Inc.: Pittsburgh, PA, 1998.
(165) Christiansen, O.; Mikkelsen, K. *J. Chem. Phys.* **1999**, *110*, 8348.
(166) Foresman, J. B.; Head-Gordon, M.; Pople, J. A.; Frisch, M. J. *J. Phys. Chem.* **1992**, *96*, 135.
(167) Stratmann, R. E.; Scuseria, G. E.; Frisch, M. J. *J. Chem. Phys.* **1998**, *109*, 8218.
(168) McDouall, J. J.; Peasley, K.; Robb, M. A. *Chem. Phys. Lett.* **1988**, *148*, 183.
(169) Dunning, T. H.; Hay, P. J. In *Methods of Electronic Structure Theory*; Schaefer, H. F., III, Ed.; Plenum Press: 1977; Vol. 3.
(170) Cossi, M.; Barone, V. *J. Phys. Chem. A* **2000**, *104*, 10614.
(171) Rittby, M.; Bartlett, R. J. *J. Phys. Chem.* **1988**, *92*, 3033.
(172) Knowles, P. J.; Hampel, C.; Werner, H.-J. *J. Chem. Phys.* **1994**, 99, 5219.
(173) Deegan, M. J. O.; Knowles, P. J. *Chem. Phys. Lett.* **1994**, *227*, 321.
(174) . Werner, H. J.; Knowles, P. J.; Almlof, J.; Amos, R. D.; Berning, A.; Cooper, D. L.; Deegan, M. J. O.; Dobbyn, A. J.; Eckert, F.; Elbert, S. T.; Hampel, C.; Lindh, R.; Lloyd, A. W.; Meyer, W.; Nicklass, A.; Peterson, K. A.; Pitzer, R. M.; Stone, A. J.; Taylor, P. R.; Mura, M. E.; Pulay, P.; Schütz, M.; Stoll, H.; Thorsteinsson, T. *MOLPRO*; Universität Stüttgart: Stüttgart, Germany; University of Birmingham: Birmingham, U.K., 2000.
(175) Anchell, J.; Apra, E.; Bernholdt, D.; Borowski, P.; Bylaska, E.; Clark, T.; Clerc, D.; Dachsel, H.; de Jong, W. A.; Deegan, M.; Dupuis, M.; Dyall, K.; Elwood, D.; Fann, G.; Fruchtl, H.; Glendenning, E.; Gutowski, M.; Harrison, R.; Hess, A.; Jaffe, J.; Johnson, B.; Ju, J.; Kendall, R.; Kobayashi, R.; Kutteh, R.; Lin, Z.; Littlefield, R.; Long, X.; Meng, B.; Nichols, J.; Nieplocha, J.; Rendall, A.; Rosing, M.; Sandrone, G.; Stave, M.; Straatsma, T.; Taylor, H.; Thomas, G.; van Lenthe, J.; Windus, T.; Wolinski, K.; Wong, A.; Zhang, Z. *NWChem*, version 4.0.1; Pacific Northwest National Laboratory: Richland, Washington, 2001.
(176) Zhan, C.-G.; Iwata, S. *Chem. Phys. Lett.* **1995**, *232*, 72.
(177) Zhan, C.-G.; Iwata, S. *J. Chem. Phys*. **1996**, *104*, 9058.
(178) Zhan, C.-G.; Iwata, S. *J. Phys. Chem. A* **1997**, *101*, 591.
(179) Zhan, C.-G.; Iwata, S. *J. Chem. Phys*. **1997**, *107*, 7323.
(180) Rienstra-Kiracofe, J. C.; Tschumper, G. S.; Schaefer, H. F., III *Chem. Rev.* **2002**, *102*, 231.
(181) Zhan, C.-G.; Nichols, J. A.; Dixon, D. A. *J. Phys. Chem. A*, accepted for publication, 2003.
(182) Gutowski, M.; Hall, C. S.; Adamowicz, L.; Hendricks, J. H.; de Clercq, H. L.; Lyapustina, S. A.; Nilles, J. M.; Xu, S.-J.; Bowen, Jr., K. H. *Phys. Chem. Lett.* **2002**, *88*, 143001.
(183) Fermi, E.; Teller, E. *Phys. Rev.* **1947**, *72*, 399.
(184) Gutowski, M.; Jordan, K. D.; Skurski, P. *J. Phys. Chem. A* **1998**, *102*, 2624.
(185) Tsurusawa, T.; Iwata, S. *J. Phys. Chem. A* **1999**, *103*, 6134.
(186) Tsurusawa, T.; Iwata, S. *J. Chem. Phys*. **2000**, *112*, 5705.
(187) Tsurusawa, T.; Iwata, S. *Adv. Metal Semicond. Clusters* **2001**, *5*, 39.
(188) Feyereisen, M. W.; Feller, D.; Dixon, D. A. *J. Phys. Chem.* **1996**, *100*, 2993.
(189) Xantheas, S. S. *J. Chem. Phys.* **1996**, *104*, 8821.
(190) Peterson, K. A.; Xantheas, S. S.; Dixon, D. A.; Dunning, T. H., Jr. *J. Phys. Chem. A* **1998**, *102*, 2449.
(191) Feller, D.; Peterson, K. A. *J. Chem. Phys.* **1999**, *110*, 8384.
(192) Feller, D. *J. Chem. Phys.* **1992**, *96*, 6104.
(193) Wagman, D. D.; Evans, W. H.; Parker, V. B.; Schumm, R. H.; Halow, I.; Bailey, S. M.; Churney, K. L.; Nutall, R. L. *J. Phys. Chem. Ref. Data* **1982**, *11*, Suppl. 2.